# Theory of the nonequilibrium structure of dense simple fluids: Effects of shearing

Hin Hark Gan and Byung Chan Eu*
*Department of Chemistry, McGill University, 801 Sherbrooke Street West, Montreal, Quebec, Canada H3A 2K6*
(Received 26 February 1991)

The nonequilibrium canonical distribution function of the generalized Boltzmann equation entails a nonequilibrium Kirkwood hierarchy of integral equations for dynamic correlation functions. A sheared simple fluid at constant density and temperature is considered. Shear effects appear in the nonequilibrum potential as additional contributions to the intermolecular potential. Approximations are introduced into the hierarchy to derive a closed integral equation for the dynamic pair-correlation function that reduces identically to the Percus-Yevick integral equation as the shear rate vanishes. Two exact results are obtained: the dynamic pair-correlation function is proven to possess the symmetry of the nonequilibrium potential, and the corresponding structure factor is shown to be positive definite for all wave-number vectors. The dynamic pair-correlation function is expanded in terms of the spherical harmonics, and the equations for coupled radial components are solved numerically. The shear rate and angular dependences of the dynamic pair-correlation function and structure factor are shown. In the low-shear-rate limit, the shear stress $P_{xy}$, pressure difference $p(\bar{\gamma})-p(0)$, and normal-stress differences $P_{yy}-P_{zz}$ and $P_{yy}-P_{zz}$ obey power laws with exponents 1, 2, and 2 respectively; $P_{xx}-P_{yy}$ is zero identically.

PACS number(s): 05.20.Dd, 05.60.+w, 05.90.+m

## I. INTRODUCTION

The structure of nonequilibrium dense fluids is of considerable experimental and theoretical interest, and its understanding is one of the important goals in nonequilibrium statistical mechanics. Experimentally, it has drawn attention from a number of directions, such as light scattering [1] from colloidal suspensions under shear, studies [2] of liquid crystal under shear, and light scattering [3] off a liquid subject to a thermal gradient. Information on the distortions of the equilibrium liquid structure can also be obtained by using computer simulations [4–6]. These phenomena, in principle, should be studied from the standpoint of nonequilibrium statistical mechanics. The difficulties associated with nonequilibrium statistical mechanics of dense fluids have impeded development in that direction. In recent years, a class of approaches broadly termed fluctuating hydrodynamics [7] have been utilized in studying problems related to the fluctuation phenomena and the question of the nonequilibrium structure of liquids. In these approaches, randomly fluctuating terms are added to the macroscopic (hydrodynamics) equations in a phenomenological way. Then, the theory of stochastic processes is used to compute various mean hydrodynamic observables and nonequilibrium fluctuations, in particular. For example, density-density correlation functions are computed, which provide nonequilibrium correlation functions and structure factors. In another approach, Hess [8] postulates a phenomenological evolution equation for the nonequilibrium correlation function, which is then suitably solved. Being phenomenological, this theory involves empirical parameters that Hess calls relaxation times. With a suitable choice of their values, the theory yields results comparable with those by computer simulations. Because of the phenomenological origin of the fluctuating terms in the fluctuating-hydrodynamic theory or the evolution equation for nonequilibrium correlation function postulated by Hess, their parentage in nonequilibrium statistical mechanics is not transparent. Moreover, in the theoretical treatment by Ronis [7(b)] and Hess [8] of the nonequilibrium distortions of the fluid structures due to shear, the equilibrium pair-correlation function is treated as an input to the equation used. Therefore, it does not form an integral part of the theory, in the sense that it is not determined by the same equation used to describe the nonequilibrium correlation function. These considerations indicate that there is a need for further studies based on nonequilibrium statistical mechanics.

It is well established that the Boltzmann equation is adequate for nonequilibrium phenomena in dilute gases, provided it is solved appropriately. On the basis of this fact and the view that dense fluid kinetic equations have a mathematical structure similar to the Boltzmann equation—the similarity principle—a generalized Boltzmann equation [9] was formulated for dense fluids. One of the principal consequences derived from the generalized Boltzmann equation is that the nonequilibrium distribution function can be written in a form similar to the canonical-ensemble distribution function, namely, an exponential form, whose exponent consists of the local equilibrium Hamiltonian and terms due to nonequilibrium contributions. The consequences of this nonequilibrium canonical distribution function together with various macroscopic equations derived from the generalized Boltzmann equation for dense fluids have been examined quite extensively by one of us (B.C.E.) in the context of irreversible thermodynamics and generalized hydrodynamics. The resulting theory is shown to conform to the second law of thermodynamics. In the generalized hydrodynamics there occur nonlinear constitutive equations for fluxes, and their implications have been tested for a

 

number of problems [10–13].

In this paper, we derive from the nonequilibrium canonical distribution function a hierarchy of nonlinear integral equations for correlation functions of various orders that describe nonequilibrium fluctuations. This approach to the structure of nonequilibrium dense fluids is similar in spirit to the theory of structure of equilibrium dense fluids [14,15]. In the equilibrium theory, the Percus-Yevick [16] (PY) and hypernetted-chain [17] equations for pair-correlation function have played an important role. In this article, we show that an integral equation for the dynamic pair-correlation function (DPCF) can be derived from the hierarchy of nonequilibrium correlation functions mentioned earlier. This integral equation reduces to the PY integral equation for the equilibrium pair-correlation function when the fluid is in equilibrium. It can also be argued that a hypernetted-chain type of integral equation is obtainable for the dynamic pair-correlation function from the hierarchy. The integral equations for the dynamic pair-correlation function suggest that the Ornstein-Zernike relation also holds for nonequilibrium fluids.

The integral equation for the dynamic pair-correlation function contains a set of macroscopic parameters $\{X^{(\alpha)}\}$ that are determined from the generalized Boltzmann equation in a manner consistent with the second law of thermodynamics. To an approximation, these parameters are proportional to macroscopic fluxes such as the heat flux, shear stress, etc. Therefore, in this approximation, the dynamic pair-correlation function is a nonlinear functional of the macroscopic fluxes. The heat flux, shear stress, etc. obey a set of evolution equations, namely, the constitutive equations, which can be derived from the generalized Boltzmann equation in a way consistent with the second law of thermodynamics. Consequently, the integral equation for the dynamic pair-correlation function is coupled to the constitutive equations for fluxes. The calculation of, for example, a dynamic structure factor requires the solution of the coupled equations, which are generally nonlinear. In this paper, we consider a nonequilibrium simple fluid undergoing a steady shear in the plane-Couette-flow geometry.

In Sec. II, the nonequilibrium Kirkwood integral equation for the dynamic correlation function, originally derived in Ref. [9(c)], is introduced. The integral equation is specialized to the case of a steady shear flow at uniform density and temperature for a non-heat-conducting fluid. Under these assumptions, the nonequilibrium Kirkwood integral equation simplifies considerably. The integral equation, which is a member of an open hierarchy of integral equations, is closed at the level of triplet-correlation function by the Kirkwood superposition approximation assumed for the dynamic triplet-correlation function. In this way, a closed integral equation is obtained for dynamic pair-correlation function. Further approximations are introduced into this integral equation that enable us to derive a new integral equation for the dynamic pair-correlation function. The resulting integral equation reduces to the well-known Percus-Yevick integral equation for the equilibrium pair-correlation function as the shear rate vanishes. In this manner, the structure of the equilibrium fluid forms an integral part of the nonequilibrium sheared fluid. A hypernetted-chain (HNC) type of integral equation will also be proposed for the dynamic pair-correlation function. These integral equations naturally satisfy a nonequilibrium Ornstein-Zernike relation, which will be made use of to obtain numerical solutions of the integral equation.

Implicit in the integral equations for the dynamic pair-correlation function is the notion of nonequilibrium potential. It contains terms from the intermolecular potential and nonequilibrium shearing effects. Given a nonequilibrium potential with an arbitrary rotational symmetry, it is proven that the dynamic pair-correlation function must possess the same symmetry. This is proven in Sec. III A. The nonequilibrium structure factor of the sheared fluid at zero wave number is related to the compressibility, which must be positive for the sheared fluid to execute a stable (steady) flow. In Sec. III B, we show that the structure factor is positive definite for all wave-number vectors for a fluid described by the integral equation for the dynamic pair-correlation function (of PY type). In Sec. IV, the dynamic pair-correlation function is solved numerically for its radial distribution functions $g_{lm}(r)$. Results for the radial distribution functions showing distortions of the equilibrium pair-correlation function are displayed and analyzed in detail in Sec. V. The shear-rate dependences of the nonvanishing harmonic components for $l=0-4$ are shown. The angular and shear-rate dependences of the (total) dynamic pair-correlation function $g(\mathbf{r})$ and structure factor $S(\mathbf{k})$ are also shown. These results are compared with those obtained from nonequilibrium-molecular-dynamics (NEMD) simulations [4]. In Sec. VI, the radial distribution functions obtained in Sec. V are used to evaluate the sheared pressure $p(\bar{\gamma})$, shear stress $P_{xy}$, and normal-stress differences $P_{xx}-P_{yy}$ and $P_{yy}-P_{zz}$. These are functions of the shear rate $\bar{\gamma}$, whose limiting power laws at low shear rates are deduced. Section VII gives a discussion and conclusions.

## II. INTEGRAL EQUATION FOR DYNAMIC PAIR-CORRELATION FUNCTION

### A. Derivation of integral equations

The theoretical basis of our development is the nonequilibrium canonical distribution function,

$$f^{(N)}(x^{(N)};t)=V^N\exp\left[-\beta\sum_{j=1}^{N}(H_j+H_j^{(1)}-m\hat{\mathcal{A}})\right], \quad (2.1)$$

which is a solution of the generalized Boltzmann equation [9] according to the modified moment method. Consequences of this form of $N$-body distribution function have been explored in the context of the kinetic theory of nonequilibrium fluids and thermodynamics of irreversible processes [9–13]. The distribution function (2.1) has been demonstrated to yield a structure of nonequilibrium thermodynamics that conforms with the laws of thermodynamics. The Hamiltonian of the $j$th particle in the frame moving with the fluid velocity $\mathbf{u}$ is

$$H_j=\tfrac{1}{2}m\mathbf{C}_j^2+\tfrac{1}{2}\sum_{k(\neq j)=1}^{N}V_{kj}\ , \tag{2.2}$$

where $\mathbf{C}_j=(\mathbf{p}_j-m\mathbf{u})/m$, $\mathbf{p}_j$ denotes the momentum of particle $j$, $m$ is the mass, and $V_{kj}$ is the intermolecular potential between particles $j$ and $k$; here we assume a pairwise additive potential. The nonequilibrium part of the Hamiltonian is a sum of contributions from all conceivable nonequilibrium processes in the system:

$$H_j^{(1)}=\sum_{\alpha}X^{(\alpha)}\odot h_j^{(\alpha)}(x^{(N)},\mathbf{u})\ , \tag{2.3}$$

where $h_j^{(\alpha)}$ are the microscopic expressions for the nonconserved variables such as the shear stress, heat flux, etc.; they are functions of the phases of $N$ particles $x^{(N)}=(\mathbf{r}^{(N)},\mathbf{p}^{(N)})$. Some relevant expressions for $h_j^{(\alpha)}$ will be explicitly written out later, but a more complete listing is found in Ref. [9(c)]. The $\{X^{(\alpha)}\}$ are unknown functions to be determined by the kinetic equation in terms of only the macroscopic observables chosen for the description of the nonequilibrium processes in the fluid. These unknowns are determined in such a way that the second law of thermodynamics is satisfied. Since they also appear in the constitutive equations for the fluxes chosen to describe the nonequilibrium evolution of the system, the entire macroscopic formulation for the system is guaranteed to satisfy the second law of thermodynamics. This is a distinctive feature of the modified moment method underlying the theory presented here. In writing down the distribution function (2.1), it is assumed that $f^{(N)}$ is normalizable. This means that if the series in Eq. (2.3) is to be truncated, it must be done such that $f^{(N)}$ is normalizable. Other symbols in Eq. (2.3) are as follows; the symbol $\odot$ stands for the scalar product between $X^{(\alpha)}$ and $h_j^{(\alpha)}$, which can be, in general, vectors or tensors. The normalization factor for $f^{(N)}$ is given by the formula

$$\exp(-\beta mN\hat{\mathcal{A}})=\frac{1}{N!h^{3N}}\int_V dx^{(N)}\exp\left[-\beta\sum_{j=1}^{N}(H_j+H_j^{(1)})\right]\ , \tag{2.4}$$

where $h$ is the Planck constant, $V$ is the volume of the system, and $\beta=1/k_BT$. The $\hat{\mathcal{A}}$ may be identified as the nonequilibrium free energy per unit mass of the fluid. In the equilibrium limit, all the nonequilibrium processes vanish, namely, $X^{(\alpha)}=0$ for all $\alpha$, and Eq. (2.1) naturally reduces to the equilibrium canonical distribution function.

The explicit microscopic expressions for the traceless symmetric and excess trace parts of the stress tensor appearing in Eq. (2.3) are

$$h_j^{(1)}=\left[m\mathbf{C}_j\mathbf{C}_j+\tfrac{1}{2}\sum_{k(\neq j)=1}^{N}F_{jk}\mathbf{r}_{jk}\mathbf{r}_{jk}\right]^{(2)} \tag{2.5}$$

and

$$h_j^{(2)}=\tfrac{1}{3}m\mathbf{C}_j^2+\tfrac{1}{6}\sum_{k(\neq j)=1}^{N}F_{jk}\mathbf{r}_{jk}\cdot\mathbf{r}_{jk}-\frac{p}{\rho}\ , \tag{2.6}$$

respectively. The symbol $[\ ]^{(2)}$ denotes the traceless symmetric part of the second-rank tensor or the dyadic, say $\mathbf{A}\mathbf{A}$:

$$[\mathbf{A}\mathbf{A}]^{(2)}=\mathbf{A}\mathbf{A}-A^2\frac{\overleftrightarrow{\mathbf{U}}}{3}\ ,$$

where $\overleftrightarrow{\mathbf{U}}$ is a unit second-rank tensor. Other notations are

$$\mathbf{r}_{jk}=\mathbf{r}_j-\mathbf{r}_k\ ,$$

$$F_{jk}=-\frac{1}{r_{jk}}\frac{\partial V(r_{jk})}{\partial r_{jk}}\ ,$$

$p$ is the hydrostatic pressure, and $\rho$ is the number density. For the purpose of the present paper, Eqs. (2.5) and (2.6) will suffice; other expressions of $h_j^{(\alpha)}$ are found in Ref. [9(c)]. These equations can be compactly written as

$$h_j^{(\alpha)}=h_{Kj}^{(\alpha)}(\mathbf{C}_j)+\sum_{k(\neq j)=1}^{N}h_{Pjk}^{(\alpha)}(x^{(N)},\mathbf{u})\ , \tag{2.7}$$

where $h_{Kj}^{(\alpha)}$ $(\alpha=1,2)$ contain all terms depending on $\mathbf{C}_j$ variables and possible constants, while $h_{Pjk}^{(\alpha)}$ contain only terms depending on the potential; the former is the kinetic part and the latter the potential part. In the absence of heat flux, it is sufficient to describe shear-related processes by keeping only the microscopic expression (2.7) for the stress tensor. In this case, the total Hamiltonian that appears in the exponent of the distribution function (2.1) can be separated into the velocity- and coordinate-dependent parts. Naturally, reduced distribution functions will be factorized into velocity- and coordinate-dependent factors. In other words, the distortion of the equilibrium distribution function in the velocity space is independent of the distortion in the coordinate space. This is also the approximation made in Ref. [18] for sheared fluids.

The nonequilibrium canonical distribution function (2.1), at a quick glance, looks like the one obtained by the maximum entropy method in information theory [19]. Despite the similarity in form, the meanings of the nonequilibrium contribution and the viewpoint taken for (2.1) and related quantities are significantly different from those taken for the exponential form derived in the maximum-entropy method. First, the nonequilibrium canonical form (2.1) does not make the entropy differential exact because of the presence of nonequilibrium fluxes. Second, the unknown functions $\{X^{(\alpha)}\}$ are determined from the generalized Boltzmann equation such that the second law of thermodynamics is strictly obeyed for all degrees of removal from equilibrium. These unknowns can, in principle, be determined to an arbitrary degree of accuracy from the set of equations generated from the generalized Boltzmann equation. In the maximum-entropy method, the $X^{(\alpha)}$ play the role of the Lagrange multipliers associated with the flux imposed as a variational constraint on the nonequilibrium entropy. Third, the fluxes obey well-defined constitutive equations derived from the generalized Boltzmann equation, whereas in the maximum-entropy method the Lagrange multipliers are computed from the constraints, namely, the statistical definition of the fluxes used as constraints.

The constraints are not evolution equations. These are significant points of departure that put the present theory apart from the entropy-maximization approach.

The pair and triplet mass density of reduced distribution functions of a single component simple fluid are defined by

$$\rho^{(2)}(\mathbf{r}_1,\mathbf{r}_2,t)=\sum_{\substack{i=1\\(i\neq j)}}^{N}\sum_{j=1}^{N}\langle m^2\delta(\mathbf{r}_i-\mathbf{r}_1)\delta(\mathbf{r}_j-\mathbf{r}_2)\times f^{(N)}(x^{(N)};t)\rangle \tag{2.8}$$

and

$$\rho^{(3)}(\mathbf{r}_1,\mathbf{r}_2,\mathbf{r}_3;t)=\sum_{\substack{i=1\\(i\neq j,j\neq k,i\neq k)}}^{N}\sum_{j=1}^{N}\sum_{k=1}^{N}\langle m^3\delta(\mathbf{r}_i-\mathbf{r}_1)\delta(\mathbf{r}_j-\mathbf{r}_2)\times\delta(\mathbf{r}_k-\mathbf{r}_3)f^{(N)}(x^{(N)};t)\rangle\ , \tag{2.9}$$

respectively. The angular brackets $\langle\cdots f^{(N)}(x^{(N)};t)\rangle$ denote an averaging over the nonequilibrium distribution function $f^{(N)}$. Higher-order reduced distribution functions are defined in a similar manner. It is also convenient to introduce the following notations:

$$\Pi^{(\alpha)}(\mathbf{r}_1,\mathbf{r}_2,\xi;t)=\frac{(Nm)^2\langle h_{P12}^{(\alpha)}(\mathbf{r}_1,\mathbf{r}_2)f^{(N)}(x^{(N)},\xi;t)\rangle_{\mathbf{r}_1\mathbf{r}_2}}{\rho^{(2)}(\mathbf{r}_1,\mathbf{r}_2,\xi;t)}\ , \tag{2.10}$$

$$\Pi^{(\alpha)}(\mathbf{r}_1,\mathbf{r}_2,\mathbf{r}_3,\xi;t)=\frac{(Nm)^3\langle h_{P12}^{(\alpha)}(\mathbf{r}_1,\mathbf{r}_2)f^{(N)}(x^{(N)},\xi;t)\rangle_{\mathbf{r}_1\mathbf{r}_2\mathbf{r}_3}}{\rho^{(2)}(\mathbf{r}_1,\mathbf{r}_2,\xi;t)}\ , \tag{2.11}$$

where $\xi$ is the charging parameter that varies from 0 to 1, and the subscripts on $\langle\ \rangle$ mean integration over all the phases except for those indicated.

An important feature of the reduced distribution functions is that they are coupled in a hierarchy. For example, $\rho^{(2)}$ is coupled to $\rho^{(3)}$, which in turn is coupled to $\rho^{(4)}$, and so on, thereby forming an open hierarchy of equations. To derive the hierarchy, the mathematical device introduced by Kirkwood [20] is employed. The derivation of the hierarchy proceeds from Eq. (2.1) in exactly the same manner as for the Kirkwood hierarchy of equilibrium correlation functions. The leading member of the hierarchy thus derived is [9(c)]

$$\begin{aligned}\frac{1}{\beta}\ln\left[\frac{\rho^{(2)}(\mathbf{r}_1,\mathbf{r}_2,\xi;t)}{\rho^{(2)}(0)}\right]&=-\xi V(\mathbf{r}_1,\mathbf{r}_2)-\int_0^{\xi}d\xi\sum_{\alpha}X^{(\alpha)}\odot\Pi^{(\alpha)}(\mathbf{r}_1,\mathbf{r}_2,\xi;t)\\&\quad-\frac{1}{m}\int_0^{\xi}d\xi\int d\mathbf{r}_3\left[V(\mathbf{r}_1,\mathbf{r}_3)\rho^{[3]}(\mathbf{r}_1,\mathbf{r}_2,\mathbf{r}_3,\xi;t)+\sum_{\alpha}X^{\alpha}\odot\Pi^{(\alpha)}(\mathbf{r}_1,\mathbf{r}_2,\mathbf{r}_3,\xi;t)\right]\\&\quad+\frac{1}{m^2N}\int_0^{\xi}d\xi\int d\mathbf{r}_1d\mathbf{r}_3\left[V(\mathbf{r}_1,\mathbf{r}_3)+\sum_{\alpha}X^{\alpha}\odot\Pi^{(\alpha)}(\mathbf{r}_1,\mathbf{r}_2,\xi;t)\right]\rho^{(2)}(\mathbf{r}_1,\mathbf{r}_2,\xi;t)\ ,\end{aligned} \tag{2.12}$$

where

$$\rho^{(2)}(0)=\rho^{(2)}(\mathbf{r}_1,\mathbf{r}_2,\xi=0;t)=(\rho^{(1)})^2 \tag{2.13}$$

and

$$\rho^{[3]}(\mathbf{r}_1,\mathbf{r}_2,\mathbf{r}_3,\xi;t)=\rho^{(3)}(\mathbf{r}_1,\mathbf{r}_2,\mathbf{r}_3,\xi;t)/\rho^{(2)}(\mathbf{r}_1,\mathbf{r}_2,\xi;t)\ . \tag{2.14}$$

The singlet distribution function $\rho^{(1)}$ $(=m\rho)$ is just the mass density of the fluid. Equation (2.12) is seen as a nonequilibrium generalization of the Kirkwood integral equation [14,20] for the equilibrium pair-distribution function in statistical mechanics. The nonequilibrium distribution function $f^{(N)}$ reduces to the equilibrium canonical distribution function as $X^{(\alpha)}\to 0$, and the nonequilibrium hierarchy (2.12) reduces to the equilibrium Kirkwood hierarchy of integral equations in the same limit.

At this stage, specialization to shear-related processes without heat conduction is made to simplify integral equation (2.12). In other words, under the assumptions stated earlier, only the $h_j^{(1)}$ and $h_j^{(2)}$ terms [of Eqs. (2.5) and (2.6), respectively] are retained. In this case, expressions in Eqs. (2.10) and (2.11) simplify, and we immediately get

$$\Pi^{(\alpha)}(\mathbf{r}_1,\mathbf{r}_2;t)=h_{P12}^{(\alpha)}(\mathbf{r}_1,\mathbf{r}_2)\ , \tag{2.15}$$

$$\Pi^{(\alpha)}(\mathbf{r}_1,\mathbf{r}_2,\mathbf{r}_3,\xi;t)=h_{P12}^{(\alpha)}(\mathbf{r}_1,\mathbf{r}_2)\rho^{[3]}(\mathbf{r}_1,\mathbf{r}_2,\mathbf{r}_3,\xi;t)\ . \tag{2.16}$$

Notice that Eq. (2.15) is actually time independent. Nonequilibrium pair- and triplet-correlation functions are related to the mass-distribution functions in Eqs. (2.8) and (2.9) as follows:

$$g^{(2)}(\mathbf{r}_1,\mathbf{r}_2,\xi;t)=\rho^{(2)}(\mathbf{r}_1,\mathbf{r}_2,\xi;t)/(m\rho)^2\ , \tag{2.17}$$

$$g^{(3)}(\mathbf{r}_1,\mathbf{r}_2,\mathbf{r}_3,\xi;t)=\rho^{(3)}(\mathbf{r}_1,\mathbf{r}_2,\mathbf{r}_3,\xi;t)/(m\rho)^3\ . \tag{2.18}$$

Further, we introduce the following definition of nonequilibrium potential:

$$V_{NE}^{*}(\mathbf{r}_1,\mathbf{r}_2;t)=\beta V(\mathbf{r}_1,\mathbf{r}_2)+\beta\sum_{\alpha=1,2}X^{(\alpha)}(t)\odot h_{P12}^{(\alpha)}(\mathbf{r}_1,\mathbf{r}_2)\ , \tag{2.19}$$

which consists of the intermolecular potential and the shear-induced terms. Here, $V_{\mathrm{NE}}^{*}$ is reduced and is thus dimensionless. The nonequilibrium Kirkwood integral equation (2.12) can be recast by using Eqs. (2.15)–(2.19); we thereby obtain

$$\ln g^{(2)}(\mathbf{r}_1,\mathbf{r}_2,\xi;t)=-\xi V^*_{\rm NE}(\mathbf{r}_1,\mathbf{r}_2;t)-\rho\int_0^\xi d\xi\int d\mathbf{r}_3 V^*_{\rm NE}(\mathbf{r}_1,\mathbf{r}_3;t)[g^{[3]}(\mathbf{r}_1,\mathbf{r}_2,\mathbf{r}_3,\xi;t)-g^{(2)}(\mathbf{r}_1,\mathbf{r}_3,\xi;t)] \tag{2.20}$$

in the thermodynamic limit, $N/V\to\rho$. This integral equation is valid for sheared incompressible fluids without heat conduction. The triplet-correlation function $g^{[3]}$ is defined by

$$g^{[3]}(\mathbf{r}_1,\mathbf{r}_2,\mathbf{r}_3,\xi;t)=g^{(3)}(\mathbf{r}_1,\mathbf{r}_2,\mathbf{r}_3,\xi;t)/g^{(2)}(\mathbf{r}_1,\mathbf{r}_2,\xi;t)\ . \tag{2.21}$$

The integral equation (2.20) is coupled to the integral equation for $g^{[3]}$, which, in turn, is coupled to the integral equation for $g^{[4]}$, and so on, thus forming an open hierarchy of coupled integral equations. This hierarchy must be suitably closed. We will introduce three approximations required to arrive at the final integral equation for the dynamic pair-correlation function. These approximations were first discussed in the context of the equilibrium Kirkwood hierarchy, where the PY integral equation was derived [21].

To close the hierarchy, we impose the Kirkwood superposition approximation for the dynamic triplet-correlation function:

$$g^{[3]}(\mathbf{r}_1,\mathbf{r}_2,\mathbf{r}_3,\xi;t)=g^{(2)}(\mathbf{r}_1,\mathbf{r}_3,\xi;t)g^{(2)}(\mathbf{r}_2,\mathbf{r}_3;t)\ . \tag{2.22}$$

This approximation may need an improvement, but any improvement gives rise to an equation significantly more complicated to solve. Since it is known to be adequate for equilibrium liquid structures, we will regard it as a first-order approximation. The dynamic pair-correlation function may be expressed in terms of the dynamic cavity function $y(\mathbf{r}_1,\mathbf{r}_2,\xi;t)$, defined by the relation

$$g^{(2)}(\mathbf{r}_1,\mathbf{r}_2,\xi;t)=\exp[-\xi V^*_{\rm NE}(\mathbf{r}_1,\mathbf{r}_2;t)]y(\mathbf{r}_1,\mathbf{r}_2,\xi;t)\ . \tag{2.23}$$

Then, as the second assumption, we vest the entire $\xi$ dependence in the Boltzmann factor in conjunction with taking $y(\mathbf{r}_1,\mathbf{r}_2,\xi=1;t)$ for the cavity function, namely,

$$g^{(2)}(\mathbf{r}_1,\mathbf{r}_2,\xi;t)=\exp[-\xi V^*_{\rm NE}(\mathbf{r}_1,\mathbf{r}_2;t)]y(\mathbf{r}_1,\mathbf{r}_2,\xi=1;t)\ . \tag{2.24}$$

This assumption presumes the cavity function to be a slowly varying function of $\xi$. The assumptions in Eqs. (2.22) and (2.24) are crucial in linking the Kirkwood hierarchy and the PY integral equation in equilibrium statistical mechanics [21]. Approximation (2.24) permits the integration of the $\xi$ parameter to be readily performed in the integral equation (2.20). We then substitute approximations (2.22) and (2.24) into integral equation (2.20) and integrate over $\xi$ to yield a closed integral equation for the dynamic cavity function:

$$\begin{aligned}\ln y(\mathbf{r}_1,\mathbf{r}_2;t)&=\rho\int d\mathbf{r}_3 f_{\rm NE}(\mathbf{r}_1,\mathbf{r}_3;t)y(\mathbf{r}_1,\mathbf{r}_3;t)\\&\quad\times\{y(\mathbf{r}_2,\mathbf{r}_3;t)[1+f_{\rm NE}(\mathbf{r}_2,\mathbf{r}_3;t)]-1\}\\&\equiv\rho P[\mathbf{r}_1,\mathbf{r}_2;t|y]\ ,\end{aligned} \tag{2.25}$$

where we have set $\xi=1$ and have defined the nonequilibrium Mayer function by

$$f_{\rm NE}(\mathbf{r}_1,\mathbf{r}_2;t)=\exp[-V^*_{\rm NE}(\mathbf{r}_1,\mathbf{r}_2;t)]-1\ . \tag{2.26}$$

Finally, integral equation (2.25) is linearized with respect to the density parameter to obtain

$$y(\mathbf{r}_1,\mathbf{r}_2;t)=1+\rho P[\mathbf{r}_1,\mathbf{r}_2;t|y]\ , \tag{2.27}$$

where $P$ is defined in Eq. (2.25). This is the principal result of this paper. As the shear rate vanishes, and hence the fluid tends to equilibrium, the integral equation (2.27) reduces to the PY integral equation, which is known to provide a sufficiently accurate description of equilibrium fluid structures. In view of this fact, this equation may be regarded as a generalization of the PY integral equation to nonequilibrium shear phenomena. It will henceforth be called the DPCF integral equation. Sources of nonequilibrium effects are contained solely in the nonequilibrium Mayer function $f_{\rm NE}$. When these effects are assumed to vanish, namely, when $X^{(\alpha)}=0$, the system returns to equilibrium. In this case, integral equation (2.27) becomes the PY integral equation for the equilibrium pair-correlation function. Thus the equilibrium structure of the fluid forms an integral part of the description of its dynamic correlations. The present approach differs from the approaches taken in Refs. [7(b)], [8], and [22] for nonequilibrium fluids, where the equilibrium structure of the fluid is treated as an input, and therefore, cannot be determined within the framework of the dynamic theory. It must be emphasized that the integral equation (2.25), within the validities of the superposition approximation and approximation (2.24), remain valid for an arbitrary strength of shear as long as $X^{(1)}$ is accurately determined from the generalized Boltzmann equation and the constitutive equation for the stress tensor is accurate. Equation (2.25) should not be regarded as being applicable in the low-shear regime only, because as far as the approximations (2.22) and (2.24) are concerned, there does not appear to be an indication that they are valid in the low-shear regime only; there is no assumption required to that effect for the derivation of Eq. (2.25).

At this point, we invoke the incompressibility assumption stated earlier and recall [9(c)] that $X^{(2)}=0$ under the assumption. This assumption simplifies the nonequilibrium potential further, which now reads

$$V^*_{\rm NE}(\mathbf{r}_1,\mathbf{r}_2;t)=\beta V(\mathbf{r}_1,\mathbf{r}_2)+\beta X^{(1)}(t):F_{12}(\mathbf{r}_{12})[\mathbf{r}_{12}\mathbf{r}_{12}]^{(2)}\ . \tag{2.28}$$

Since $X^{(1)}$ is proportional to the shear stress [see Eq. (2.35) below], the second term on the right is the shear-induced effect, which is a source of anisotropy. The anisotropy of the nonequilibrium potential is reminiscent of angle-dependent intermolecular potentials for molecular fluids [23], where the angular dependence originates from

the orientations of nonspherical molecules. Because of this mathematical similarity, the methodology of obtaining the solutions of integral equation (2.27) is similar to that used in solving for the structure of dense molecular fluids, as will be seen in Sec. IV. As noted earlier, $X^{(1)}$ should be determined from the generalized Boltzmann equation for dense fluids [9(b),9(c)]. Given an approximate solution of $X^{(1)}$ from the kinetic equation, the DPCF integral equation can be solved for $y(\mathbf{r},t)$ at various densities, temperatures, and shear rates. By virtue of the neglect of heat flux in the problem, the system under consideration is homogeneous in temperature.

It is easy to verify that the DPCF integral equation (2.27) can be written in the form of the time-dependent Ornstein-Zernike relation

$$h(\mathbf{r},t)=c(\mathbf{r},t)+\rho\int d\mathbf{r}'c(\mathbf{r}-\mathbf{r}',t)h(\mathbf{r}',t) , \tag{2.29}$$

where the time-dependent direct correlation function has the form of the PY closure in equilibrium fluids:

$$c_{\mathrm{PY}}(\mathbf{r},t)=f_{\mathrm{NE}}(\mathbf{r},t)y(\mathbf{r},t) . \tag{2.30}$$

In Eq. (2.29), $\mathbf{r}=\mathbf{r}_1-\mathbf{r}_2$ and $h(\mathbf{r},t)=g^{(2)}(\mathbf{r},t)-1$. Since the nonequilibrium contribution enters the problem through the nonequilibrium Mayer function, it is also justified to propose a HNC-type closure,

$$c_{\mathrm{HNC}}(\mathbf{r},t)=h(\mathbf{r},t)-\ln y(\mathbf{r},t) , \tag{2.31}$$

for nonequilibrium sheared fluids. For fluids with a long-range potential, this closure is seen as more appropriate than closure (2.30), just as in equilibrium fluids. In the $k$ space, the time-dependent Ornstein-Zernike relation reads

$$\tilde{h}(\mathbf{k},t)=\frac{\tilde{c}(\mathbf{k},t)}{1-\rho\tilde{c}(\mathbf{k},t)} , \tag{2.32}$$

and the time-dependent structure factor is given by the formula

$$S(\mathbf{k},t)=1+\rho\tilde{h}(\mathbf{k},t) . \tag{2.33}$$

Relation (2.29) or (2.32) with closure (2.30) is equivalent to integral equation (2.27). This relation will be used to solve the DPCF integral equation in Sec. IV. Once the integral equation is solved for $\tilde{h}$, the structure factor is obtained from Eq. (2.33).

### B. Plane Couette flow

We consider a plane Couette flow where the fluid confined between two parallel infinite plates is sheared. The plates are aligned parallel to the $x$ axis and are separated by a distance $D$ in the $y$ direction. The $z$ direction is, therefore, neutral. The plates at $y=\pm D/2$ move at velocities $\pm u_0/2$, in opposite directions along the $x$ axis. This means that the velocity field of the flow is $\mathbf{u}=u_0yD^{-1}\hat{\mathbf{e}}_x$, where $\hat{\mathbf{e}}_x$ is the unit vector along the $x$ axis. In this case, the $x$-$y$ plane defines the shear plane, and the nonvanishing shear stress is the $xy$ component. The DPCF integral equation contains macroscopic variables, the shear stress in the present case, through $X^{(1)}$. The evolution equation (constitutive equation) for shear stress can be derived [10] from the generalized Boltzmann equation in full generality. The constitutive equation obtained has been used to examine [10,24], quite successfully, the rheological properties of various fluids which becomes non-Newtonian at high shear rates. If the shear rates are low or moderate and the normal stress effects are neglected because they are known to be second-order effects, the constitutive equation, which is generally nonlinear, for shear stress becomes the Maxwell equation [25]. For the present problem, the Maxwell equation takes the form

$$\frac{\partial P_{xy}}{\partial t}=-2p\gamma-\Omega P_{xy} , \tag{2.34}$$

where $P_{xy}$ is the $xy$ component of the traceless symmetric shear stress, $\gamma$ is the shear rate defined by $\gamma=2^{-1}(\partial u_x/\partial y)$, $\Omega=p/\eta_0$, where $p$ is the hydrostatic pressure, and $\eta_0$ is the shear viscosity; $\Omega^{-1}$ is the relaxation time for shear stress. We remark that the constitutive equation should be at least corotational if the normal stresses are adequately taken into account [10]. Since the present work aims to illustrate the utility of the present theory in a manner as simple as possible, the normal stresses are neglected. In the steady-state limit, the shear stress is given by the Newtonian formula $P_{xy}=-2\eta_0\gamma$, implying that $\eta_0$ is a Newtonian viscosity. This viscosity can, in principle, be calculated from its statistical mechanical formula given in Ref. [9(b)], but it will be treated as an empirical parameter in this work, since its evaluation is not the aim of this paper. For a fluid not too far from equilibrium, $X^{(1)}$ is proportional to the shear stress [10,24(c)]:

$$X^{(1)}=-\frac{P_{xy}}{2p} . \tag{2.35}$$

For a liquid, the shear stress described by Eq. (2.34) relaxes fairly quickly to its steady-state value predicted by the Newtonian formula. Since we are interested in a steady-shearing experiment here, it is permissible to take the Newtonian formula for $P_{xy}$, so $X^{(1)}$ is written in the form

$$X^{(1)}=\frac{\eta_0\gamma}{p} . \tag{2.36}$$

More generally, for non-Newtonian fluids, the Maxwell equation is replaced by a more-suitable constitutive equation. Such constitutive equations can be found in Refs. [9(b)], [10], [24], and [25]. The shear viscosity becomes $\gamma$ dependent in this case. It has now become apparent from the integral equation (2.27), the definition of the nonequilibrium potential (2.28), and relation (2.36) that the dynamic pair-correlation function is a nonlinear functional of the shear stress. The non-Newtonian fluid will be considered in a sequel to this paper.

To fix the coordinate system, we denote the polar angle between a vector and the $z$ axis by $\theta$ and the azimuthal angle around the $z$ axis by $\phi$. The shear $xy$ plane lies on the plane of $\theta=\pi/2$. From the definition of $V^*_{\mathrm{NE}}$ [Eq. (2.28)] and relation (2.36), the nonequilibrium potential in the chosen coordinate system is given by

$$V^*_{\rm NE}(r,\theta,\phi)=V^*(r)-\frac{\eta_0\gamma}{p}r\frac{\partial V^*(r)}{\partial r}\sin2\phi\sin^2\theta\ . \quad (2.37)$$

We choose the soft-sphere intermolecular potential $V^*=\beta\epsilon r^{-12}$, where $r$ is a reduced radial distance $R/\sigma$, with $\sigma$ being the effective diameter of the molecule, and the parameter $\beta\epsilon$ is set equal to unity (see Fig. 1). The shear effect should diminish in the hard-core region ($r<1$). This is satisfied when $V^*_{\rm NE}\geq 0$, or, more specifically, when the normalized shear rate $\bar{\gamma}$ is less than unity:

$$\bar{\gamma}=\frac{12\eta_0\gamma}{p}<1\ . \quad (2.38)$$

Limiting $\bar{\gamma}$ to low values is consistent with the use of the Maxwell equation to obtain the shear stress. In the present calculation of sheared fluids, condition (2.38) marks the range of validity of approximations (2.34) and (2.36). When these approximations are replaced by more-accurate ones, the range of the allowed values of $\bar{\gamma}$ can be extended.

We will now obtain approximate solutions of the DPCF integral equation (2.27) for a fluid undergoing a steady shear. The first iterative solution of integral equation (2.27) is given by

$$y(\mathbf{r})=1+\rho P[\mathbf{r}|y_0]\ , \quad (2.39)$$

where the equilibrium cavity function $y_0(r)$ is to be obtained from the PY integral equation. We then use the definition of the dynamic cavity function [Eq. (2.23)] and the nonequilibrium potential [Eq. (2.28)] to obtain an approximate dynamic pair-correlation function

$$g(r,\theta,\phi)=g_0(r)\exp(-\bar{\gamma}r^{-12}\sin2\phi\sin^2\theta)\ , \quad (2.40)$$

where $g_0(r)$ is the equilibrium pair-correlation function. The shear viscosity of the fluid is taken from NEMD simulations [26] of the same soft-sphere potential $V^*(r)=r^{-12}$. At packing fraction $\eta\approx 0.45$, the viscosity has the value $\eta_0=1.5(m\epsilon)^{1/2}\sigma^{-2}$. If we define the dimensionless variables $\gamma^*=\sigma\gamma(m/\epsilon)^{1/2}$ and $p^*=p\sigma^3/\epsilon$, the reduced shear rate is given by $\bar{\gamma}=18\gamma^*/p^*$. Then $p^*\approx 10$ at packing fraction $\eta=0.45$, so $\bar{\gamma}\approx 2\gamma^*$.

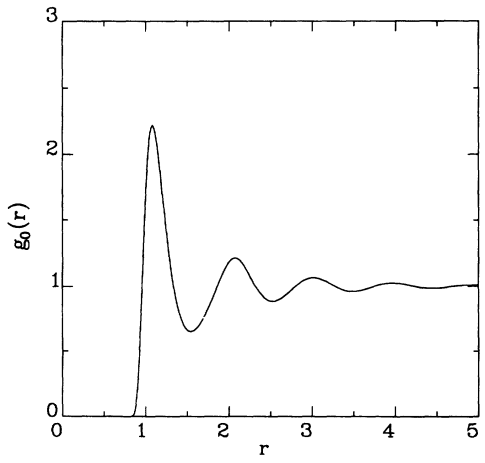


FIG. 1. Equilibrium pair-correlation function of a simple fluid with soft-sphere potential $V^*=\beta\epsilon r^{-12}$, where $\beta\epsilon=1$. The result is from the Percus-Yevick integral equation at packing fraction $\eta=0.45$. The variable $r$ is a reduced radial distance $R/\sigma$.

The dynamic pair-correlation function of the first iterative solution vanishes in the core region because of condition (2.38) and the presence of the factor $g_0(r)$; it approaches $g_0(r)$ for $r\gg 1$. Because of the $r^{-12}$ radial dependence in its exponent, significant nonequilibrium distortions in $g(\mathbf{r})$ are confined to the vicinity of $r=1$. In this approximation, $g(\mathbf{r})$ is still nonlinear in the shear rate. The nonequilibrium factor of solution (2.40) is also density dependent through the Newtonian viscosity $\eta_0$. Outside of the hard core ($r>1$), the linearized solution

$$g(r,\theta,\phi)=g_0(r)\left[1-\frac{\bar{\gamma}}{r^{12}}\sin2\phi\sin^2\theta\right] \quad (2.41)$$

is a good approximation to the first iterative solution (2.40). In terms of the spherical harmonics, the new solution is given by

$$g(r,\theta,\phi)=\sqrt{4\pi}g_0(r)\{Y_{00}+(i\bar{\gamma}/r^{12})\sqrt{\tfrac{2}{15}}\times[Y_{22}(\theta,\phi)-Y^*_{22}(\theta,\phi)]\}\ , \quad (2.42)$$

where $i$ is an imaginary number. Evidently, only $l=0$ and 2 harmonics are retained in the linearized solution. It will be shown in Sec. IV that these are also the dominant harmonics contributing to the nonequilibrium distortions of equilibrium pair-correlation function. The angular dependence of solution (2.41) is identical with the Stokes approximation [26]. This result has also been obtained by other authors [7(b),8] who have used different approaches.

## III. EXACT RESULTS

### A. Symmetry of the dynamic pair-correlation function

The nonequilibrium potential $V^*_{\rm NE}(\mathbf{r}_1,\mathbf{r}_2;t)$ [of Eq. (2.28)] may possess certain symmetry properties depending on the system under consideration. In equilibrium simple fluids, $V^*(r)$ has radial symmetry or rotational invariance. It is evident that the equilibrium pair-correlation function has the same symmetry regardless of the integral equation it satisfies. For nonequilibrium fluids, the relationship between the symmetry of the nonequilibrium potential $V^*_{\rm NE}$ and dynamic pair-correlation function $g(\mathbf{r}_1,\mathbf{r}_2;t)$ needs to be established. It will be proven in the following that for an arbitrary rotational symmetry of $V^*_{\rm NE}(\mathbf{r}_1,\mathbf{r}_2;t)$, the dynamic pair-correlation function $g(\mathbf{r}_1,\mathbf{r}_2;t)$ has the same rotational symmetry.

Nonlinear integral equations satisfied by the dynamic pair-correlation function can be generally written as

$$g(\mathbf{r}_1,\mathbf{r}_2)=L[\mathbf{r}_1,\mathbf{r}_2|g,f_{\rm NE}]\ . \quad (3.1)$$

$L$ is a function of the variables $\mathbf{r}_1$ and $\mathbf{r}_2$ through the function $g(\mathbf{r}_1,\mathbf{r}_2)$ and the nonequilibrium Mayer function $f_{\rm NE}(\mathbf{r}_1,\mathbf{r}_2)$. The time variable is suppressed because it does not affect the arguments to follow. In principle, Eq. (3.1) can be rearranged so that $g(\mathbf{r}_1,\mathbf{r}_2)$ is expressible in terms of $f_{\rm NE}(\mathbf{r}_1,\mathbf{r}_2)$ functions only. Formally, it reads

$$g(\mathbf{r}_1,\mathbf{r}_2)=M[\mathbf{r}_1,\mathbf{r}_2|f_{\rm NE}] , \tag{3.2}$$

where $M$ is a functional of $f_{\rm NE}$, or, equivalently, $V^*_{\rm NE}$. An example of Eq. (3.2) would be the cluster expansion of the dynamic pair-correlation function, which is easily performed by iterating integral equation (3.1) in a fashion similar to equilibrium fluids. We assume that the nonequilibrium potential $V^*_{\rm NE}$ or $f_{\rm NE}$ is dependent only on the molecular variable $\mathbf{r}=\mathbf{r}_1-\mathbf{r}_2$. This is certainly the case with the nonequilibrium potential (2.37) for sheared fluids described in Sec. II B. Suppose the function $f_{\rm NE}$ has an arbitrary rotational symmetry:

$$\mathcal{R}f_{\rm NE}(\mathbf{r})=f_{\rm NE}(\mathcal{R}\mathbf{r})=f_{\rm NE}(\mathbf{r}) , \tag{3.3}$$

where $\mathcal{R}$ is a rotation operator [27]. The same rotation operator $\mathcal{R}$ operates on $g(\mathbf{r}_1,\mathbf{r}_2)$; we have, from Eq. (3.2),

$$\mathcal{R}g(\mathbf{r}_1,\mathbf{r}_2)=g(\mathcal{R}\mathbf{r}_1,\mathcal{R}\mathbf{r}_2)=M[\mathcal{R}\mathbf{r}_1,\mathcal{R}\mathbf{r}_2|f_{\rm NE}] . \tag{3.4}$$

We can also define a new function $\mathcal{M}$ to be related to the function $M$ in the following way:

$$M[\mathcal{R}\mathbf{r}_1,\mathcal{R}\mathbf{r}_2|f_{\rm NE}] = \int d\mathbf{r}'\mathcal{M}[f_{\rm NE}(\mathcal{R}\mathbf{r}_1-\mathbf{r}'),f_{\rm NE}(\mathcal{R}\mathbf{r}_2-\mathbf{r}')] . \tag{3.5}$$

It is permissible to write $M$ in this form because it is strictly a functional of $f_{\rm NE}$ functions. Since $\mathbf{r}'$ is an integration variable, the following change of variable is allowed:

$$\mathbf{r}'\rightarrow\mathcal{R}\mathbf{r}' , \tag{3.6}$$

$$d\mathbf{r}'\rightarrow d(\mathcal{R}\mathbf{r}') . \tag{3.7}$$

With this change of variable, Eq. (3.5) then reads

$$M[\mathcal{R}\mathbf{r}_1,\mathcal{R}\mathbf{r}_2|f_{\rm NE}] = \int d(\mathcal{R}\mathbf{r}')\mathcal{M}[f_{\rm NE}(\mathcal{R}(\mathbf{r}_1-\mathbf{r}')),f_{\rm NE}(\mathcal{R}(\mathbf{r}_2-\mathbf{r}'))] . \tag{3.8}$$

Since the Jacobian of rotational transformation is equal to unity and $f_{\rm NE}$ has rotational invariance [Eq. (3.3)], we conclude, from Eqs. (3.4) and (3.8), that

$$\mathcal{R}g(\mathbf{r}_1,\mathbf{r}_2)=M[\mathbf{r}_1,\mathbf{r}_2|f_{\rm NE}]=g(\mathbf{r}_1,\mathbf{r}_2) , \tag{3.9}$$

i.e., $g(\mathbf{r}_1,\mathbf{r}_2)$ possesses the same rotational symmetry of the nonequilibrium potential $V^*_{\rm NE}$ described by the rotation operator $\mathcal{R}$. To reiterate the requirements for the validity of the proof, we require the nonequilibrium potential to be a function of the molecular variable $\mathbf{r}$ and that the integral equation (3.1) be expressible as a functional of the nonequilibrium potential only. Both requirements are clearly satisfied in a sheared simple fluid. The symmetry property of the dynamic pair-correlation function will be useful in constraining the number of solutions needed to solve the integral equation it satisfies and in explaining various features of dynamic structures obtained from it.

### B. Positivity of the dynamic structure factor

The dynamic structure factor can be shown [15] to be related to the scattering cross section in the perturbative approximation, and it is therefore a positive quantity. This is a constraint that must be satisfied by the solutions of the integral equation obeyed by the dynamic pair-correlation function. For a fluid undergoing a steady plane Couette flow, which is described by the DPCF integral equation (2.27) or Eq. (2.29) with closure (2.30), the positivity of its structure factor can be shown. The steady-state structure factor is given by

$$S(\mathbf{k})=\frac{1}{1-\rho\tilde{c}(\mathbf{k})} . \tag{3.10}$$

In a plane Couette flow, described in Sec. II B, the nonequilibrium potential has inversion symmetry. Accordingly, the dynamic pair-correlation function also possesses inversion symmetry from the result of Sec. III A. The dynamic cavity and direct correlation function then have inversion symmetry:

$$\begin{aligned} y(\mathbf{r})&=y(-\mathbf{r}) , \\ c(\mathbf{r})&=c(-\mathbf{r}) . \end{aligned} \tag{3.11}$$

Furthermore, physical requirements dictate that

$$y(\mathbf{r})\geq 0 . \tag{3.12}$$

It holds trivially when $y(\mathbf{r})$ satisfies the nonequilibrium Kirkwood integral equation (2.20) or the HNC-type integral equation [(2.29) with closure (2.31)]. Inequality (3.12) will hold for integral equation (2.27) or Eq. (2.29) with closure (2.30) in the domain of fluid densities, as is the case with the PY integral equation for equilibrium fluids.

From its definition in Eq. (3.10), the structure factor is obviously positive when $\rho=0$. To prove that it is also positive when $\rho>0$, it is sufficient to prove the inequality

$$1-\rho\tilde{c}(\mathbf{k})>0 , \tag{3.13}$$

where

$$-\rho\tilde{c}(\mathbf{k})=-\rho\int d\mathbf{r}e^{i\mathbf{k}\cdot\mathbf{r}}c(\mathbf{r}) . \tag{3.14}$$

The $\tilde{c}(\mathbf{k})$ function is an example of a multivariate characteristic function. Its Taylor expansion in variables $(k_1,k_2,k_3)$, referring to $(x,y,z)$ components of $\mathbf{k}$, is given by

$$-\rho\tilde{c}(\mathbf{k})=-\rho\tilde{c}(0)\sum_{m_1,m_2,m_3}\frac{(ik_1)^{m_1}(ik_2)^{m_2}(ik_3)^{m_3}}{m_1!m_2!m_3!} \times\mu_{m_1m_2m_3} , \tag{3.15}$$

where the moments are defined by

$$\mu_{m_1,m_2,m_3}=\int_{-\infty}^{\infty}dx\int_{-\infty}^{\infty}dy\int_{-\infty}^{\infty}dz\,x^{m_1}y^{m_2}z^{m_3}\times[c(x,y,z)/\tilde{c}(0)]\ , \tag{3.16}$$

and $m_i=0,1,2,\ldots$. Since $c(x,y,z)$ is even in its arguments [Eq. (3.11)], the moments are nonzero only when $m_1$, $m_2$, and $m_3$ take zero or even-integer values. The function $-\rho\tilde{c}(\mathbf{k})$ of Eq. (3.15) can be rewritten in terms of its cumulants [28]:

$$-\rho\tilde{c}(\mathbf{k})=-\rho\tilde{c}(0)\exp\left[\sum_{m_1,m_2,m_3}{}'\frac{(ik_1)^{m_1}(ik_2)^{m_2}(ik_3)^{m_3}}{m_1!m_2!m_3!}\times\kappa_{m_1m_2m_3}\right], \tag{3.17}$$

where the prime on the summation means that the indices are not all zero simultaneously. The cumulants are defined by

$$\kappa_{m_1m_2m_3}=\langle x^{m_1}y^{m_2}z^{m_3}\rangle=\frac{\partial^{m_1}}{\partial k_1^{m_1}}\frac{\partial^{m_2}}{\partial k_2^{m_2}}\frac{\partial_{m_3}}{\partial k_3^{m_3}}F(\mathbf{k})\bigg|_{\mathbf{k}=0}, \tag{3.18}$$

where

$$F(\mathbf{k})=\ln[\tilde{c}(\mathbf{k})/\tilde{c}(0)]\ . \tag{3.19}$$

Since $F(\mathbf{k})$ is even in all of its arguments, only those cumulants with indices having zero or even integers are nonzero. This means that the exponent of Eq. (3.17) is real and that the exponential factor itself is, therefore, positive. To complete the proof, we have to show that $-\rho\tilde{c}(0)$ is positive. We use the definition of $\tilde{c}(0)$ and closure (2.30) to obtain a bound for $-\rho\tilde{c}(0)$:

$$-\rho\tilde{c}(0)=-\rho\int d\mathbf{r}c(\mathbf{r})=-\rho\int d\mathbf{r}f_{\rm NE}(\mathbf{r})y(\mathbf{r})=\rho\int d\mathbf{r}|f_{\rm NE}(\mathbf{r})|y(\mathbf{r})>0\ . \tag{3.20}$$

The third equality holds because of the restriction that $f_{\rm NE}\le 0$ or $V_{\rm NE}^{*}\ge 0$ [see the discussion following Eq. (2.37)], the condition $y(\mathbf{r})\ge 0$, and the fact that the integrand is not zero everywhere. Equations (3.17) and (3.20) imply that the bound (3.13) is satisfied; consequently, the structure factor is positive for $\rho>0$. Since this also holds when $\rho=0$, we conclude that $S(\mathbf{k})$ is positive definite for all physical fluid densities. When the intermolecular potential has an attractive tail, say, the Leonard-Jones potential, the nonequilibrium potential is no longer repulsive everywhere. In this case, the integrand $-f_{\rm NE}(\mathbf{r})y(\mathbf{r})$ is not strictly positive everywhere, but its mean may still be positive. This is almost certainly assured because $-f_{\rm NE}$ is positive in the core region ($r<1$) and approaches zero rapidly outside this region, where the attractive potential becomes effective.

## IV. HARMONIC DECOMPOSITION OF THE DPCF INTEGRAL EQUATION

The DPCF integral equation (2.27) satisfies the nonequilibrium Ornstein-Zernike relation with closure (2.30). We find it more efficient to solve the integral equation in the form of the Ornstein-Zernike relation than the integral equation itself. We first write the Ornstein-Zernike relation in $k$ space:

$$\tilde{h}(\mathbf{k})=\tilde{c}(\mathbf{k})+\rho\tilde{c}(\mathbf{k})\tilde{h}(\mathbf{k})\ . \tag{4.1}$$

The function $\tilde{h}(\mathbf{k})$ can be expanded in terms of a complete set of spherical harmonics:

$$\tilde{h}(\mathbf{k})=\sum_{l=0}^{\infty}\sum_{m=-l}^{l}\tilde{h}_{lm}(k)Y_{lm}(\hat{\mathbf{k}})\ , \tag{4.2}$$

where $\hat{\mathbf{k}}$ is a unit wave-number vector. The $\tilde{c}(\mathbf{k})$ function can be similarly expanded in terms of the spherical harmonics. On using the harmonic expansions of $\tilde{h}(\mathbf{k})$ and $\tilde{c}(\mathbf{k})$, we obtain the $(l_3m_3)$ component of the Ornstein-Zernike relation from Eq. (4.1) by using standard manipulations of the spherical harmonics:

$$\tilde{h}_{l_3m_3}(k)=\tilde{c}_{l_3m_3}(k)+\rho\sum_{\substack{l_1l_2\\ m_1,m_2}}Q(l_1l_2l_3;m_1m_2m_3)\tilde{c}_{l_1m_1}(k)\times\tilde{h}_{l_2m_2}(k)\ , \tag{4.3}$$

where the coefficients

$$Q(l_1l_2l_3;m_1m_2m_3)=\int d\hat{\mathbf{k}}\,Y_{l_1m_1}(\hat{\mathbf{k}})Y_{l_2m_2}(\hat{\mathbf{k}})Y_{l_3m_3}^{*}(\hat{\mathbf{k}})=\left[\frac{2l_1+1)(2l_2+1)}{4\pi(2l_3+1)}\right]^{1/2}\times C(l_1l_2l_3;000)\times C(l_1l_2l_3;m_1m_2m_3)\ . \tag{4.4}$$

The $C(l_1l_2l_3;m_1m_2m_3)$ are the Clebsch-Gordan coefficients [29,23]; they are zero when $m_3\neq m_1+m_2$. As the sheared fluid approaches equilibrium, the shear rate vanishes, and, consequently, all harmonic components tend to zero except for the (00) component, leaving only one equation to solve.

In the plane Couette flow under consideration, the function $h(\mathbf{r})$ has the following symmetries:

$$h(x,y,z)=h(-x,-y,-z)\ , \tag{4.5}$$

$$h(x,y,z)=h(-x,-y,z)\ , \tag{4.6}$$

which are also the symmetries of the nonequilibrium potential. These symmetries restrict the harmonic components $h_{lm}(r)$ to having only even $l$ and $m$ indices. It can be readily shown that the same symmetries hold for $\tilde{h}(\mathbf{k})$ and likewise for $\tilde{c}(\mathbf{k})$. Furthermore, since $\tilde{h}(\mathbf{k})$ and $\tilde{c}(\mathbf{k})$ are real functions, we have the symmetry relations

$$\tilde{h}_{lm}(k)=\tilde{h}^{*}_{l-m}(k)\ ,\qquad \tilde{c}_{lm}(k)=\tilde{c}^{*}_{l-m}(k) \tag{4.7}$$

for even $l$ and $m$; the asterisk denotes complex conjugation. Let us define a new function

$$\tilde{q}_{l_3m_3}(k)=\tilde{h}_{l_3m_3}(k)-\tilde{c}_{l_3m_3}(k) . \tag{4.8}$$

We further define functions with their equilibrium values subtracted out as follows:

$$\begin{aligned}\tilde{q}^{(1)}_{lm}(k)&=\tilde{q}_{lm}(k)-\tilde{q}^{(0)}(k)\delta_{l0}\delta_{m0} ,\\ \tilde{c}^{(1)}_{lm}(k)&=\tilde{c}_{lm}(k)-\tilde{c}^{(0)}(k)\delta_{l0}\delta_{m0} ,\end{aligned} \tag{4.9}$$

where the superscript (0) denotes the equilibrium value of the function. It is convenient to define two-dimensional matrices whose elements are

$$\tilde{K}((l_3m_3)(l_2m_2);k)=\sum_{l_1,m_1} Q(l_1l_2l_3;m_1m_2m_3)\tilde{c}_{l_1m_1}(k) , \tag{4.10}$$

$$\begin{aligned}\tilde{K}^{(1)}&((l_3m_3)(l_2m_2);k)\\ &=\sum_{l_1,m_1} Q(l_1l_2l_3;m_1m_2m_3)\\ &\quad\times\{[\tilde{q}^{(0)}(k)+2\tilde{c}^{(0)}(k)]\delta_{l_10}\delta_{m_10}+\tilde{c}_{l_1m_1}(k)\} .\end{aligned} \tag{4.11}$$

Here, $(l_3m_3)$ is the row index of the matrix, and $(l_2m_2)$ is the column index. In terms of the new functions, i.e., Eqs. (4.9), (4.10), and (4.11), the integral Eq. (4.3) cast in the matrix form reads

$$\tilde{\mathbf{q}}^{(1)}=\rho[\vec{U}-\rho\tilde{\mathbf{K}}]^{-1}\tilde{\mathbf{K}}^{(1)}\tilde{\mathbf{c}}^{(1)} , \tag{4.12}$$

where $\tilde{\mathbf{q}}$, $\tilde{\mathbf{K}}$, $\tilde{\mathbf{K}}^{(1)}$, and $\tilde{\mathbf{c}}^{(1)}$ are matrices whose elements have been defined. The right-hand side is small at low shear rates, even at high densities, because $\tilde{c}^{(1)}_{lm}(k)$ is small. The solution of Eq. (4.1) is now reduced to solving the matrix equation (4.12). In principle, the matrix equation is infinite dimensional and therefore must be truncated in numerical computations. The convergence of the solution as a result of considering a finite-dimensional matrix equation can be checked by increasing the dimension of the matrix equation.

We still have to write the closure (2.30) in terms of the spherical harmonics. The direct correlation function in the configuration space can be written as

$$c(\mathbf{r})=[1+q(\mathbf{r})]f_{\rm NE}(\mathbf{r}) , \tag{4.13}$$

where $q(\mathbf{r})=h(\mathbf{r})-c(\mathbf{r})$. The harmonic components of $c(\mathbf{r})$ are given by

$$\begin{aligned}c_{l_3m_3}(r)=&\sum_{\substack{l_1l_2\\ m_1m_2}} Q(l_1l_2l_3;m_1m_2m_3)\\ &\times[1+q(\mathbf{r})]_{l_1m_1}f_{l_2m_2}(r) .\end{aligned} \tag{4.14}$$

where $[1+q(\mathbf{r})]_{l_1m_1}$ denotes the $(l_1m_1)$ component of $[1+q(\mathbf{r})]$. The function $f_{lm}(r)$ is the radial component of $f_{\rm NE}(\mathbf{r})$, and it is fixed when the nonequilibrium potential is given. It can be shown that for even $l$ and $m$,

$$\begin{aligned}f_{lm}(r)&=e^{-V^*(r)}\int d\hat{\mathbf{r}}\, e^{-\delta V^*_{\rm NE}(r)}Y_{lm}(\hat{\mathbf{r}})-\sqrt{4\pi}\delta_{l0}\delta_{m0}\\ &=\eta_{lm}e^{-V^*(r)}\int_0^1 dx\, P_{lm}(x)I_{m/2}(z)\\ &\quad-\sqrt{4\pi}\delta_{l0}\delta_{m0} ,\end{aligned} \tag{4.15}$$

where the variable $z$ is defined by

$$z=-\frac{\bar{\gamma}}{r^{12}}(1-x^2)$$

and the coefficient $\eta_{lm}$ by

$$\eta_{lm}=\frac{4\pi}{i^{m/2}}\left[\frac{(2l+1)(l-m)!}{4\pi(l+m)!}\right]^{1/2} .$$

The $\hat{\mathbf{r}}$ is a unit vector in the coordinate space; $P_{lm}(x)$ are the associated Legendre polynomials, and $I_{m/2}$ are the modified Bessel functions; $\delta V^*_{\rm NE}$ denotes the shear part of the nonequilibrium potential [see Eq. (2.37)].

The functions $c^{(1)}_{lm}(r)$ are obtained from $c_{lm}(r)$ of Eq. (4.14) and the known equilibrium function $c^{(0)}(r)$. Since the equation (4.12) to be solved is in $k$ space, we will need to evaluate $c_{lm}(r)$ in $k$ space, and similarly for $\tilde{q}_{lm}(k)$. The forward and inverse transforms for the $q$ function are given by

$$\tilde{q}_{lm}(k)=4\pi i^l\int_0^\infty dr\, r^2 j_l(kr)q_{lm}(r) \tag{4.16}$$

and

$$q_{lm}(r)=\frac{(-i)^l}{2\pi^2}\int_0^\infty dk\, k^2 j_l(kr)\tilde{q}_{lm}(k) , \tag{4.17}$$

respectively. These are simply the forward and inverse Hankel transforms. The transform pairs of other functions are defined in a similar manner.

The scheme of our numerical computation consists of iterating Eq. (4.12) together with closure (4.14). The linearized solutions of the functions $h_{lm}(r)$ and $c_{lm}(r)$ are used to initiate the iteration. Their explicit expressions will be given below. The required transforms to go from the configuration space to the $k$ space and vice versa are given by Eqs. (4.16) and (4.17). In actual numerical implementations, the transforms are not calculated according to these expressions except for the case $l=0$, where they are just the Fourier transforms. For the $l\neq 0$ cases, the Hankel transforms are recast into expressions involving Fourier transforms, which are more suitable for numerical computations. The details involved are nontrivial, but they are entirely technical in nature. We refer the reader to Refs. [30] and [23] for the details. The scheme of computation of the structure of sheared fluids presented here is analogous to the calculation of the structures of equilibrium molecular fluids [23,31]. Lado's method [32] of performing the three-dimensional Fourier transform was used throughout. It is essentially exact for the numerical parameters we chose. The numerical parameters are the maximum (reduced) radial distance $R_{\rm max}$ and the grid size $\Delta R$. According to Lado's prescription for the Fourier transform, the corresponding parameters in $k$ space are $\Delta k=\pi/R_{\rm max}$ and $k_{\rm max}=N\Delta k$, where $N=R_{\rm max}/\Delta R$ is the total number of points. We set

$R_{\max}=10$ and $\Delta R=0.05$ unless indicated otherwise. This choice ensures that the radial distribution functions are accurate to three significant figures at all points. For example, in the hard-core region, $g_{lm}(r<0.5)<10^{-3}$. Typically, this accuracy required about 500 iterations for packing fraction $\eta=0.45$.

The initial values of the radial distribution functions are obtained from the linearized solutions of $h_{lm}(r)$ and $c_{lm}(r)$. The contributing harmonic components of $h(\mathbf{r})$ are obtained from Eq. (2.42):

$$h_{00}^{(0)}(r)=\sqrt{4\pi}[g_0(r)-1]\ ,$$
$$h_{22}^{(0)}(r)=\left[\frac{8\pi}{15}\right]^{1/2}(i\bar{\gamma})\frac{g_0(r)}{r^{12}}\ , \tag{4.18}$$
$$h_{2-2}^{(0)}(r)=[h_{22}^{(0)}(r)]^*\ ;$$

other components ($l>2$) are zero. The superscript (0) denotes initial guessed values, and $g_0(r)$ is the equilibrium pair-correlation function. The approximate $c_{lm}(r)$ are deduced by linearizing closure (4.13) with respect to the shear rate $\bar{\gamma}$. We obtain

$$c_{00}^{(0)}(r)=\sqrt{4\pi}c_0(r)\ ,$$
$$c_{22}^{(0)}(r)=\left[\frac{8\pi}{15}\right]^{1/2}(i\bar{\gamma})\frac{g_0(r)}{r^{12}}\ , \tag{4.19}$$
$$c_{2-2}^{(0)}(r)=[c_{22}^{(0)}(r)]^*\ .$$

All other components are again zero, and $c_0(r)$ is the equilibrium direct correlation function obtained from the solution of the PY equation.

## V. NUMERICAL RESULTS

The DPCF integral equation (2.27), together with the method of solution presented in Sec. IV, allows a systematic examination of nonequilibrium effects in the structure of sheared simple fluids. In particular, the temperature, density, and shear-rate dependences of the distortions of the dynamic pair-correlation function can be studied. For a given temperature, density, and shear rate, the relative importance of the harmonic components can be evaluated. In this work, we study the shear-rate dependence of the sheared simple fluid structure at a sufficiently high density, $\eta=0.45$, as is done in NEMD simulations [4]. The temperature scale is controlled by $\beta\epsilon$, which has been set equal to unity for simplicity. The shear-rate dependence of the dynamic pair-correlation function has recently been extensively studied by Hanley *et al.* [4(a)] using NEMD simulations. However, this work is limited to two-dimensional sheared simple fluids. Even so, many of its qualitative features are similar to the three-dimensional results obtained here. Some results for three-dimensional simple fluids have also been reported [4(d)]. The works just cited will be used for comparison with the results obtained here.

Calculations were performed at three shear rates: $\bar{\gamma}=0.25$, 0.5, and 0.75. At each shear rate, truncation at $l_{\max}=4$ was imposed, and higher-harmonic components, $l=6$, 8, 10, etc., were regarded as small. For the shear rates considered here, this is indeed justified. The harmonic components $g_{lm}(r)$ were found to be either real (Re) or imaginary (Im) and never fully complex; the $g_{l-m}(r)$ components are simply the complex conjugate of $g_{lm}(r)$. Figure 2 shows $\mathrm{Re}(g_{00})/\sqrt{4\pi}$ as a function of the radial distance $r$ at shear rates $\bar{\gamma}=0.25$ (dash-dotted curve), 0.5 (dashed curve), and 0.75 (solid curve). The most noticeable behaviors in Fig. 2 are the distortions at the maxima and minima of $\mathrm{Re}(g_{00})$. The magnitudes of the distortions decrease with increasing distance from the core region ($r<1$). Increasing the shear rate appears to have the effect of decreasing the density, inasmuch as the amplitudes of the oscillations tend to be reduced at the extrema. Another prominent feature is the node structure of the curves at different shear rates. The nodes occur along $\mathrm{Re}[g_{00}(r)]/\sqrt{4\pi}=1$. In the two-dimensional NEMD simulations of Ref. [4(a)], the scalar component $g_s$ exhibits all the features related to the shear-rate dependence of $\mathrm{Re}(g_{00})$. As the shear rate increases, the curve of $\mathrm{Re}(g_{00})$ tends to move into the hard-core region, but the effect is not significant. This effect arises because the core of the nonequilibrium potential $V_{\mathrm{NE}}^*$ [Eq. (2.37)] softens when $\bar{\gamma}$ is close to 1.

The node structure and the decrease of the amplitudes of oscillations with increasing distance observed in the shear-rate dependence of $\mathrm{Re}(g_{00})$ are also seen in the higher-harmonic components, $g_{lm}$ for $l>0$. Figures 3–7 show the curves of $g_{lm}$ for $l=2$–4. For $l>0$ cases, most significant contributions occur around $r=1$, but persistent oscillations are seen at least up to $r=5$. These are non-negligible long-range effects due to shearing that are not seen in the linearized approximation (2.42). The

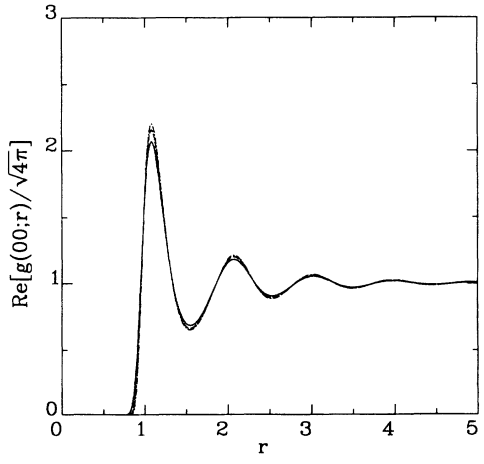


FIG. 2. The dynamic pair-correlation function of a fluid undergoing a steady plane Couette flow is shown. Results were obtained by solving Eq. (2.27) numerically. The curves correspond to the radial harmonic component $\mathrm{Re}(g_{00}/\sqrt{4\pi})$ at different shear rates: $\bar{\gamma}=0.25$ (dash-dotted curve), 0.50 (dashed curve), and 0.75 (solid curve). All results are at packing fraction $\eta=0.45$.

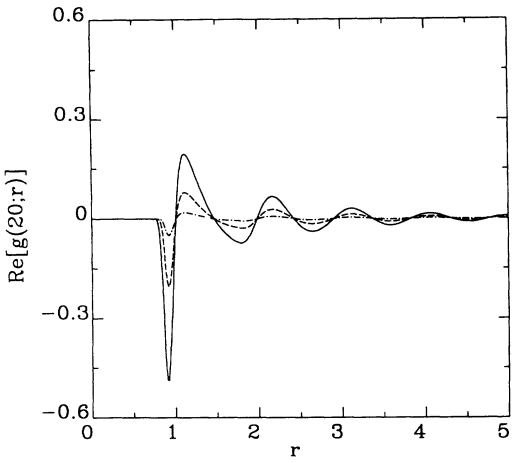


FIG. 3. Same as in Fig. 2 but for the radial function $\mathrm{Re}[g_{20}(r)]$.

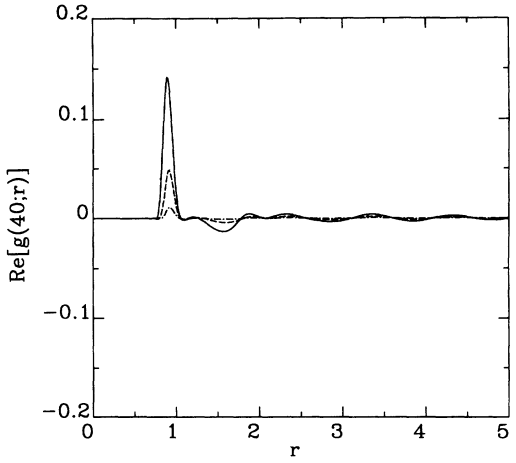


FIG. 5. Same as in Fig. 2 but for the radial function $\mathrm{Re}[g_{40}(r)]$.

nonequilibrium distortion of the equilibrium pair-correlation function due to the $\mathrm{Im}(g_{22})$ component (in Fig. 4) is always larger than the $\mathrm{Re}(g_{20})$ component (in Fig. 3) at all shear rates. In fact, the first peaks of $\mathrm{Im}(g_{22})$ are three times larger in magnitude than the corresponding peaks of $\mathrm{Re}(-g_{20})$. The $\mathrm{Re}(g_{40})$ (Fig. 5) and $\mathrm{Im}(g_{42})$ (Fig. 6) components are comparable in magnitude, but they are about an order of magnitude smaller than the $\mathrm{Im}(g_{22})$ component. The first minima of the $\mathrm{Re}(g_{44})$ component (in Fig. 7) are comparable in magnitude to the corresponding minima of the $\mathrm{Re}(g_{20})$ component, but the amplitudes of the other extrema are much smaller in magnitude. It is interesting that the linearized solution in Eq. (2.42) already contains $\mathrm{Re}(g_{00})$ and $\mathrm{Im}(g_{22})$ components. As can be seen in Figs. 2 and 4, these are also the most significant nonequilibrium distortions in the dynamic pair-correlation function. However, in the linearized solution, $\mathrm{Re}(g_{00})$ is independent of shear rate.

The angular dependence of the (total) dynamic pair-correlation function is another important feature of sheared fluids. We recall that the nonequilibrium potential is rendered anisotropic by the shear-induced term. As a result, the dynamic pair-correlation function is angle dependent. The nature of this dependence at different shear rates can be understood by examining the nonequilibrium potential. We will show the angular dependence of $g(\mathbf{r})$ at a fixed shear rate ($\bar{\gamma}=0.75$) and its shear-rate dependence at a fixed angle ($\phi=3\pi/4$). In Fig. 8, the angular dependence of the dynamic pair-correlation function $g(r,\theta=\pi/2,\phi)$ in the shear plane is shown at a fixed shear rate $\bar{\gamma}=0.75$. In terms of its harmonic components,

$$g(r,\theta=\pi/2,\phi)=\sum_{l,m} g_{lm}(r)Y_{lm}(\theta=\pi/2,\phi)\ . \tag{5.1}$$

The curves at $\phi=0$ and $\pi/2$ (solid curves) exactly overlap. This is due to the symmetry of the nonequilibrium potential

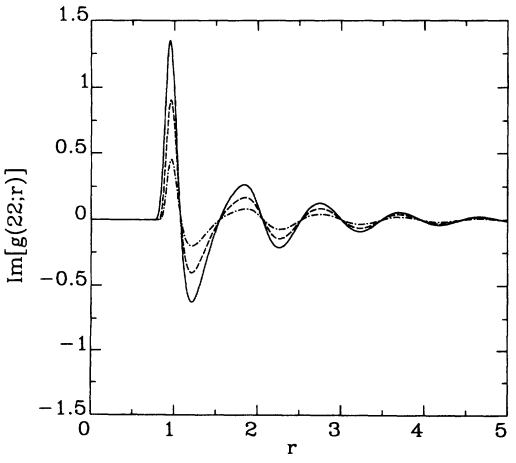


FIG. 4. Same as in Fig. 2 but for the radial function $\mathrm{Im}[g_{22}(r)]$.

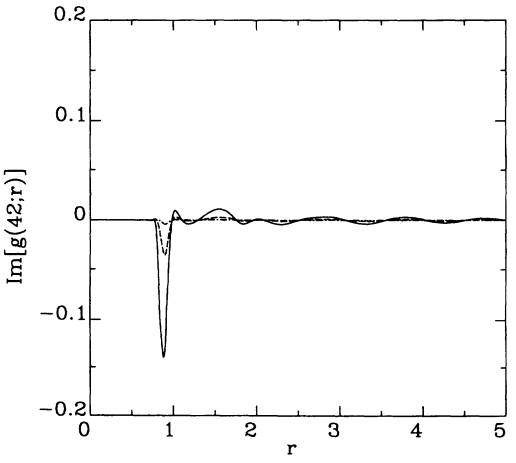


FIG. 6. Same as in Fig. 2 but for the radial function $\mathrm{Im}[g_{42}(r)]$.

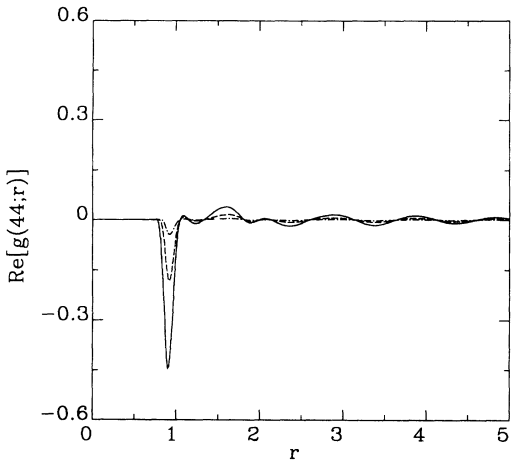


FIG. 7. Same as in Fig. 2 but for the radial function $\mathrm{Re}[g_{44}(r)]$.

$$V^*_{\mathrm{NE}}(r,\theta=\pi/2,\phi=0)=V^*_{\mathrm{NE}}(r,\theta=\pi/2,\phi=\pi/2)\ . \quad (5.2)$$

The curves of $g(r,\theta=\pi/2,\phi)$ are also shown at angles $\phi=\pi/4$ (dash-dotted curve) and $3\pi/4$ (dashed curve). In the former case the dominant peak is positioned just outside of the hard core ($r>1$), whereas in the latter case it is positioned just inside of the hard core. These features can be accounted for by evaluating the nonequilibrium potential at the angles of interest. The shear-induced term of the nonequilibrium potential has a $\sin 2\phi$ angular dependence in the shear plane ($\theta=\pi/2$). At angles $\phi=0$ and $\pi/2$, this term vanishes. Since at $\phi=\pi/4$ it gives a positive contribution, the nonequilibrium potential becomes more repulsive than the $\phi=0$ or $\pi/2$ case. Consequently, the dominant peak of the curve at $\phi=\pi/4$ is positioned outside of the hard core ($r>1$), as shown in Fig. 8. At $\phi=3\pi/4$, the shear-induced term gives a negative contribution, thereby weakening the nonequilibrium potential in the hard core; hence the observed opposite effect. In addition, the dominant peaks at different angles have different heights, with the $\phi=3\pi/4$ case higher than the $\phi=\pi/4$ case, which in turn is higher than the $\phi=0$ and $\pi/2$ cases. The overall features of these curves are similar to the results provided by the NEMD simulations [4(a)] in two dimensions. In this connection, we remark that the dynamic pair-correlation function for sheared fluids obtained from Hess's equation reads [8]

$$g(\mathbf{r})=\int_0^\infty d\alpha\, e^{-\alpha} g_0(x-\alpha\bar{\gamma}y,y,z)\ , \quad (5.3)$$

where $\bar{\gamma}$ is the normalized shear rate and $g_0$ is the equilibrium pair-correlation function. We have evaluated Eq. (5.3) for $\bar{\gamma}=0.75$ at $\eta=0.45$, using the Percus-Yevick solution for $g_0(r)$. The relative positions of the first peak of $g(r,\theta=\pi/2,\phi)$ at different values of $\phi$ are the same as those we have obtained. However, numerical solutions show that $g(\mathbf{r})$ is significantly different from zero in the hard-core region ($r<1$). Computer simulations [4(a)] do not show such behavior, however. This difficulty can be identified by examining the behavior of Eq. (5.3) in the core region. Furthermore, the first peak of $g(r,\theta=\pi/2,\phi=\pi/4)$ is higher than $g(r,\theta=\pi/2,\phi=3\pi/4)$, which is not seen in NEMD simulations and our calculations.

In Fig. 9, the shear-rate dependence of the total pair-correlation function $g(r,\theta=\pi/2,\phi)$ at $\phi=3\pi/4$ is shown. The solid curve corresponds to zero shear rate, and the dash-dotted and dashed curves are for shear rates $\bar{\gamma}=0.5$ and 0.75, respectively. As the shear rate is increased, the repulsiveness of the nonequilibrium potential is progressively weakened, thereby causing the curves to move further into the core region. The opposite is true at $\phi=\pi/4$, as can be deduced from the nonequilibrium potential. A similar analysis can be made for the dynamic structure factor.

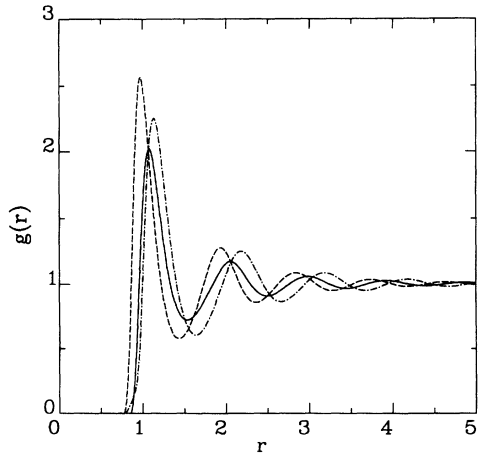


FIG. 8. The angular dependence of the total dynamic pair-correlation function $g(r,\theta=\pi/2,\phi)$ [see Eq. (5.1)] at shear rate $\bar{\gamma}=0.75$ is shown. The curves shown are at angles $\phi=0$ (solid curve), $\pi/4$ (dash-dotted curve), $\pi/2$ (solid curve), and $3\pi/4$ (dashed curve). All results are at packing fraction $\eta=0.45$.

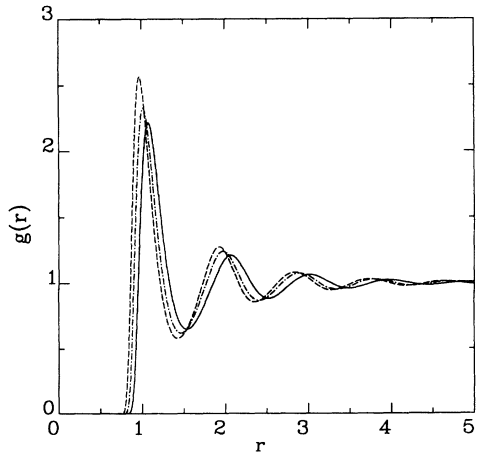


FIG. 9. The shear-rate dependence of the total dynamic pair-correlation function $g(r,\theta=\pi/2,\phi)$ at angle $\phi=3\pi/4$ is shown. The cases shown are at shear rates $\bar{\gamma}=0$ (solid curve), 0.5 (dash-dotted curve), and 0.75 (dashed curve). All results are at packing fraction $\eta=0.45$.

The nonequilibrium structure factor in terms of the spherical harmonics is written as

$$S(k,\theta_k,\phi_k)=1+\rho\sum_{l,m}S_{lm}(k)Y_{lm}(\theta_k,\phi_k)\ , \tag{5.4}$$

where its radial distribution functions in terms of $h_{lm}(r)$ are

$$S_{lm}(k)=4\pi i^l\int_0^\infty dr\, r^2 j_l(kr)h_{lm}(r)\ . \tag{5.5}$$

The azimuthal angle $\phi_k$ is defined to be in the $k_x-k_y$ plane, and $\theta_k$ refers to the polar angle. Structure factors in the shear plane ($\theta_k=\pi/2$) at angles $\phi_k=0,\pi/2$ (solid curve), $\phi_k=\pi/4$ (dash-dotted curve), and $\phi_k=3\pi/4$ (dashed curve) are displayed in Fig. 10. The shear rate is fixed at $\bar{\gamma}=0.75$. These curves are equivalent to the curves of Fig. 8 but in the reciprocal $k$ space. The structure factors are positive at all angles ($\phi$) and $k$ values shown. This is a numerical confirmation of the positivity of the structure factor of sheared simple fluids, proven analytically in Sec. III B. Some insignificant numerical noise is seen in the low-wave-number region, however. As is the case in the configuration space, the structure factors in the $k_x-k_y$ plane at angles $\phi_k=0$ and $\pi/2$ (solid) curves are the same. The curve at $\phi_k=\pi/4$ (dash-dotted curve) is moved to the left of the $\phi_k=0$ curve, to the lower-wave-number region, whereas the curve at the $\phi_k=3\pi/4$ (dashed) curve is moved to the higher-wave-number region. Since the structure factor is related to the differential cross section, its angular dependence can be explained in terms of the collision mechanism of the molecules. The structure factor at $\phi_k=\pi/4$ samples molecules interacting at larger distances than those sampled at $\phi_k=3\pi/4$ because its main contribution is in the lower-wave-number region or lower momentum transfer. The shear-rate dependence of the structure factors, in the shear plane, at $\phi_k=3\pi/4$ is shown in Fig. 11.

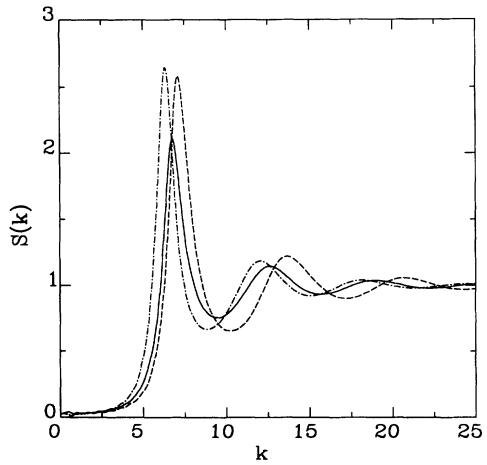


FIG. 10. The angular dependence of the structure factor $S(k,\theta_k=\pi/2,\phi_k)$ [see Eq. (5.4)] at shear rate $\bar{\gamma}=0.75$ is shown as a function of the wave number $k$. The curves shown are at angles $\phi_k=0$ (solid curve), $\pi/4$ (dash-dotted curve), $\pi/2$ (solid curve), and $3\pi/4$ (dashed curve). All results are at packing fraction $\eta=0.45$.

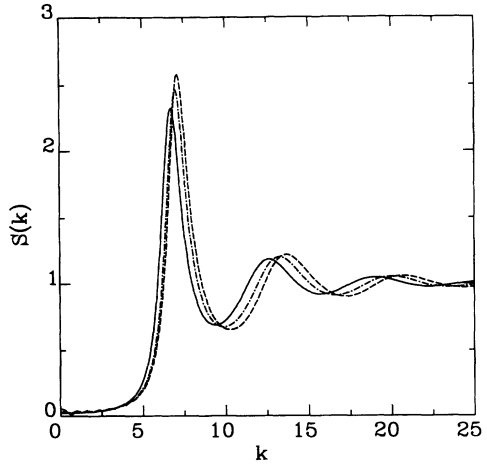


FIG. 11. The shear-rate dependence of the structure factor $S(k,\theta_k=\pi/2,\phi_k=3\pi/4)$ is shown as function of the wave number $k$ in the shear plane. The cases shown are at shear rates $\bar{\gamma}=0$ (solid curve), 0.5 (dash-dotted curve), and 0.75 (dashed curve). All results are at packing fraction $\eta=0.45$.

The solid curve refers to $\bar{\gamma}=0$, the dash-dotted curve to $\bar{\gamma}=0.5$, and the dashed curve to $\bar{\gamma}=0.75$. Increasing the shear rate has the effect of moving the extrema of the structure factor at $\phi_k=3\pi/4$ toward the higher-wave-number or frequency region. The opposite effect was found to be the case for the structure factor at $\phi_k=\pi/4$. In summary, the nonequilibrium potential plays a vital role in accounting for the observed features of the nonequilibrium structures, which are qualitatively in accord with computer simulations. In the present theory, the nonequilibrium potential determines the nature of nonequilibrium effects.

## VI. PRESSURE AND NORMAL-STRESS DIFFERENCES

The thermodynamics functions of sheared fluids close to equilibrium can be constructed from the structural information obtained from the DPCF integral equation (2.27). The functions may include the nonequilibrium pressure tensor, internal energy, compressibility, etc. Determination of the shear-rate dependence of these functions will yield information about the macroscopic state of the sheared fluid as it is gradually removed from equilibrium. The results for the shear-rate dependence of the pressure tensor are available from the three-dimensional NEMD simulation [33], mode-coupling calculations [34], and kinetic theory [35]. We evaluate the pressure tensor of the sheared fluid in the following.

The pressure tensor for a steady sheared fluid is given by [36]

$$\overleftrightarrow{P}=\frac{\rho}{\beta}\overleftrightarrow{U}-\frac{\rho^2}{2}\int d\mathbf{r}\frac{\mathbf{rr}}{r}\frac{\partial V(r)}{\partial r}g(\mathbf{r})\ . \tag{6.1}$$

where $g(\mathbf{r})$ is the dynamic pair-correlation function of the sheared fluid. The dynamic pair-correlation function is determined by the DPCF integral equation (2.27). In a

simple shear flow, the relevant quantities are the pressure $p$, shear stress $P_{xy}$, and normal-stress difference. For the soft-sphere potential assumed, they are written in terms of $g_{lm}(r)$ as

$$\frac{\beta}{\rho}\Delta p(\bar{\gamma})=\frac{\beta}{\rho}[p(\bar{\gamma})-p(0)] =8\pi\rho\int_0^\infty dr\, r^{-10}\left[\frac{g_{00}(r)}{\sqrt{4\pi}}-g_0(r)\right], \tag{6.2}$$

$$\frac{\beta}{\rho}P_{xy}=\left[\frac{6\pi}{5}\right]^{1/2}4\rho\int_0^\infty dr\, r^{-10}\mathrm{Im}[g_{22}(r)], \tag{6.3}$$

$$\frac{\beta}{\rho}(P_{xx}-P_{yy})=\left[\frac{6\pi}{5}\right]^{1/2}8\rho\int_0^\infty dr\, r^{-10}\mathrm{Re}[g_{22}(r)], \tag{6.4}$$

$$\frac{\beta}{\rho}(P_{yy}-P_{zz})=-\left[\frac{\pi}{5}\right]^{1/2}12\rho \times\int_0^\infty dr\, r^{-10}\{g_{20}(r)+\sqrt{\tfrac{2}{3}}\mathrm{Re}[g_{22}(r)]\}. \tag{6.5}$$

Other components of the tensor do not contribute because the symmetry of the shear flow admits only even-$m$ values. Since the pressure tensor (6.1) is of rank 2, only $l=0$ and 2 components of $g_{lm}$ are involved in Eqs. (6.2)–(6.5). The (primary) normal stress difference in Eq. (6.4) vanishes because $\mathrm{Re}(g_{22})=0$. This is due to the symmetry of the nonequilibrium potential; it depends only on the $xy$ and $r$ variables. Accordingly, $g^{(2)}$ depends on the same variables. Then, by using the symmetry of $g^{(2)}$ and Eq. (6.1) to evaluate $P_{xx}$ and $P_{yy}$, we see that these diagonal tensor components are the same. Three-dimensional NEMD simulations [4(d)] indicate that $\mathrm{Re}(g_{22})\neq 0$. Thus $P_{xx}\neq P_{yy}$ in general for non-Newtonian fluids. This defect of the present calculation can be rectified by using constitutive equations that are more general than the Maxwell equation. The remaining nonvanishing quantities are Eqs. (6.2), (6.3), and (6.5); Eq. (6.5) is sometimes called the secondary normal-stress difference [25].

Associated with the thermodynamic functions in Eqs. (6.2), (6.3), and (6.5), there are three coefficients characterizing the macroscopic state of the sheared fluid [30]:

$$\Delta p(\bar{\gamma})=4D(\bar{\gamma})\bar{\gamma}^2, \tag{6.6}$$

$$P_{xy}=-2\bar{\eta}(\bar{\gamma})\bar{\gamma}, \tag{6.7}$$

$$P_{yy}-P_{zz}=-4\Psi(\bar{\gamma})\bar{\gamma}^2. \tag{6.8}$$

The numerical factors appear on the right-hand side of these equations because of our definition of $\bar{\gamma}$. The coefficients $D$, $\bar{\eta}$, and $\Psi$ in general depend on the shear rate $\bar{\gamma}$, density $\rho$, and temperature $\beta$. Since $\rho$ and $\beta$ are fixed for all shear rates in the sheared system considered, the coefficients can vary with $\bar{\gamma}$ only. The coefficient $D(\bar{\gamma})$ is identified as the dilatancy factor due to shear, and coefficient $\bar{\eta}(\bar{\gamma})$ is the non-Newtonian shear viscosity.

It is instructive to compare the shear-rate dependence of the coefficients obtained from the linearized solution [Eq. (2.42)] with those from the numerical solutions of the DPCF integral equation (2.27). We recall that the linearized solution retains only the $g_{00}$, $g_{22}$, and $g_{2-2}$ harmonic components. In this approximation, $g_{00}$ is independent of $\bar{\gamma}$, so $D=0$ from Eq. (6.2). The $g_{22}$ or $g_{2-2}$ component is linear in shear rate $\bar{\gamma}$, and this means $\bar{\eta}$ is a constant or it is a Newtonian viscosity. Finally, $\Psi$ is clearly zero because the $g_{20}$ component does not contribute to the linearized solution. Hence, the linearized solution has the consequence that the fluid is Newtonian.

Figure 12 shows the numerical results for the curves of the thermodynamic functions versus shear rate, constructed from the solutions of the DPCF integral equation (2.27). The curves of $\Delta p(\bar{\gamma})$ (solid curve), $P_{xy}/4$ (dashed curve), and $P_{yy}-P_{zz}$ (dash-dotted curve) versus $\bar{\gamma}$ are shown on a $\log_{10}$-$\log_{10}$ graph; all curves are scaled by a factor $\beta/\rho$. The range of the shear rate covers two decades, $10^{-2}\leq\bar{\gamma}<1$. For $\bar{\gamma}>0.5$, the radial distribution functions $g_{lm}$ were calculated to an accuracy of three significant figures, as was the case with all the calculations reported in Sec. V. When $\bar{\gamma}<0.5$, the thermodynamic functions of Eqs. (6.6)–(6.8) acquire small values, thus requiring them to be computed with greater accuracy. We increased the accuracy of $g_{lm}$ to 4–5 significant figures. This was achieved with a finer grid size, $\Delta R=0.025$, and greater cutoff radius, $R_{\max}=15$. The curves of the functions in Eqs. (6.6)–(6.8) are linear on the $\log_{10}$-$\log_{10}$ graph for $\bar{\gamma}<0.3$. This implies that they obey power laws. The quantities $\Delta p$ and $P_{yy}-P_{zz}$ have the same slope of 2, whereas $P_{xy}$ has a slope of 1; they obey, respectively, quadratic and linear laws in the low-shear-rate limit. The exponent for $\Delta p(\bar{\gamma})$, however, is at variance with the value obtained by NEMD simula-

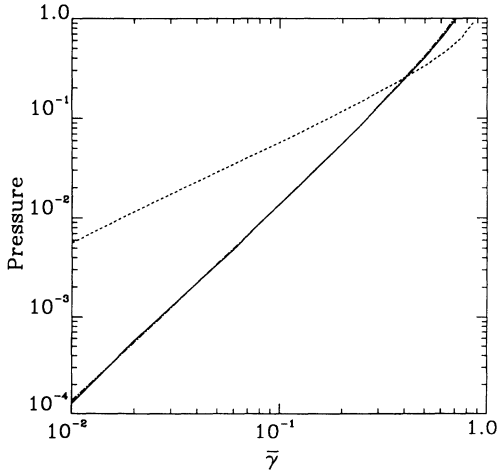


FIG. 12. The shear-rate dependence of the pressure difference $\Delta p(\bar{\gamma})$ (solid curve), shear stress $P_{xy}/4$ (dashed curve), and normal stress difference $P_{yy}-P_{zz}$ (dash-dotted curve) are shown; the curves are scaled by a factor $\beta/\rho$. These results were obtained from Eqs. (6.2), (6.3), and (6.5). All results are at packing fraction $\eta=0.45$.

tions, which gives 1.5 while our value is 2. Thus, from expressions (6.6)–(6.8), the coefficients $D$, $\Psi$, and $\bar{\eta}$ are found to be constant functions. The constancy of the viscosity coefficient with respect to the shear rate again implies that it is Newtonian.

The limiting power laws for the thermodynamic functions (6.6)–(6.8) can be demonstrated analytically if the first iterative solution [Eq. (2.40)] is assumed to be a good approximation in the low-shear-rate limit. We expand $g(\mathbf{r})$ in terms of the shear-rate parameter $\bar{\gamma}$ to get

$$g(r,\theta,\phi)=\sqrt{4\pi}g_{00}(r) \times[Y_{00}-\bar{\gamma}A(r,\theta,\phi) +(\bar{\gamma}^2/2!)A^2(r,\theta,\phi)-\cdots], \quad (6.9)$$

where

$$A(r,\theta,\phi)=(-i/r^{12})\sqrt{\tfrac{2}{15}}[Y_{22}(\theta,\phi)-Y_{2-2}(\theta,\phi)] . \quad (6.10)$$

This expansion is then substituted into Eq. (6.1). To obtain Eqs. (6.2)–(6.5), the appropriate components of Eq. (6.1) are selected. We then use the orthogonality of the spherical harmonics and a property of the Clebsch-Gordan coefficients; i.e., they vanish for $m_3 \neq m_1+m_2$ [see definition (4.4)]. The leading corrections for $\Delta p(\bar{\gamma})$ and $P_{yy}-P_{zz}$ due to nonequilibrium effects are found to be quadratic in $\bar{\gamma}$, whereas it is linear for the shear stress $P_{xy}$. Hence an approximate analytical analysis of the relevant stress tensor components reproduces the shear-rate dependence of the thermodynamic functions in the low-shear-rate limit, as shown in Fig. 12.

## VII. DISCUSSION AND CONCLUSION

The theory of the structure of nonequilibrium dense fluids presented in this article was developed in parallel with the theory of equilibrium fluids. This was made possible by the nonequilibrium canonical distribution function for nonequilibrium simple fluids. Given the nonequilibrium canonical distribution function, the procedure used to derive [9(c)] the integral equations for the dynamic pair-correlation function is analogous to that used in equilibrium fluids [14,20]. In fact, the parallelism is so close that the integral equations obtained suggest the generalization of the Ornstein-Zernike relation for equilibrium fluids to nonequilibrium situations. The connection between the equilibrium and nonequilibrium integral equations is made through the nonequilibrium potential. When the nonequilibrium terms in the aforementioned potential are taken to vanish, the equilibrium integral equations are recovered identically. The proof of the equivalence of the symmetry properties of the nonequilibrium potential and the dynamic pair-correlation function provides an efficient way of specifying the symmetry of the dynamic pair-correlation function. It can, therefore, be exploited to constrain the number of (independent) solutions needed to be solved from the DPCF integral equation. The positivity of the structure factor of sheared fluids corresponding to the DPCF integral equation (2.27) was shown under general conditions. Numerical solutions of the DPCF integral equation (2.27) confirmed the analytic demonstration of the positivity of structure at all shear rates and angles considered. Systematic tools were then set up to solve the DPCF integral equation (2.27). We have used expansions in the spherical harmonics to reduce the integral equation into single-variable coupled equations of the radial distribution functions in the reciprocal space. The adequacy of truncating the expansion at $l_{\max}=4$ was tested numerically for all shear rates considered, $\bar{\gamma}<1$.

A significant limitation in the calculations ought to be noted. Use was made of the Maxwell equation for shear stress, which, by definition, is valid only for fluids near equilibrium, hence the constraint on the range of the shear rate, $\bar{\gamma}<1$. This limitation can be easily removed by using a more adequate equation for stress tensor [9(b)] that is valid for fluids far from equilibrium. The dense-fluid kinetic equation, on which the present work is based, has provided constitutive equations that can adequately describe nonlinear fluid properties, such as non-Newtonian viscosities of complex fluids. These constitutive equations can be applied to study nonequilibrium structures of fluids far from equilibrium. Extensions can also be made by considering a more-accurate form of $X^{(\alpha)}$. This would require more elaborate solutions from the kinetic equation. Another important extension of the calculations presented in this paper is the inclusion of the heat-flux term in the nonequilibrium potential. It will enable us to treat nonuniformity in temperature that may arise from the presence of heat fluxes at boundaries and the unavoidable thermoviscous effect in a sheared system. The scope of the theory presented in Sec. II is sufficiently general to encompass such extensions.

The $N$-body distribution function of the modified moment method has a form similar to that of the maximum entropy method [19]. However, the macroscopic fluxes $X^{(\alpha)}$ are determined in a different way. In the present theory, they are determined by an underlying kinetic equation to any degree of accuracy desired, in such a manner that they are consistent with the exponential form of the distribution function. In this sense, the distribution function of the modified moment method is, in principle, capable of describing systems that are far from equilibrium. The velocity distribution function of the maximum entropy method for a dilute gas has been compared with molecular-dynamics simulations [37]. This aspect of simulation data may also be examined by using the modified moment method, but the focus of the present work has been the correlation of particles in the configuration space.

The radial harmonic components of the dynamic pair-correlation function obtained from the DPCF integral equation enabled us to evaluate the pressure tensor components of the sheared fluid. From these tensor components, the shear-rate dependences of the pressure-related thermodynamic functions were deduced. They were found to obey integral power laws in the low-shear-rate limit. The theory developed in this paper provides a relatively economic alternative, albeit an approximate one, to numerical-simulation methods, and therefore may

be used as a qualitative guide to more-elaborate numerical methods. Its more practical utility probably lies in the direction of using the DPCF integral equation for investigations of quantities less accessible to numerical simulations, such as dynamics of phase transitions. The integral equation has the potential of being as useful as its equilibrium counterpart, the Percus-Yevick equation.

## ACKNOWLEDGMENTS

The present work is supported in part by the Natural Sciences and Engineering Research Council of Canada and Fonds FCAR of Quebec. We thank David Ronis for discussions.

---

*Also at the Physics Department, McGill University, Montreal, Quebec, Canada H3A 2T8.

[1] N. A. Clark and B. J. Ackerson, Phys. Rev. Lett. **44**, 1005 (1980); B. J. Ackerson and N. A. Clark, Physica A **118**, 221 (1983).

[2] U. D. Kini, J. Phys. (Paris) Colloq. **40**, C3-62 (1979), and many other papers in the issue.

[3] D. Beysens, Y. Garrabos, and G. Zalczer, Phys. Rev. Lett. **45**, 403 (1980).

[4] (a) H. J. M. Hanley, G. P. Morriss, T. R. Welberry, and D. J. Evans, Physica A **149**, 406 (1988); (b) J. C. Rainwater, H. J. M. Hanley, and S. Hess, Phys. Lett. A **126**, 150 (1988); (c) H. J. M. Hanley, J. C. Rainwater, and S. Hess, Phys. Rev. A **36**, 1795 (1987); (d) H. J. M. Hanley, J. C. Rainwater, N. A. Clark, and B. J. Ackerson, J. Chem. Phys. **79**, 4448 (1983).

[5] J. J. Erpenbeck, Phys. Rev. Lett. **52**, 1333 (1984).

[6] W. Xue and G. S. Grest, Phys. Rev. Lett. **64**, 419 (1990).

[7] See, for example, (a) A. M. S. Tremblay, M. Arai, and E. D. Siggia, Phys. Rev. A **23**, 1451 (1981); (b) D. Ronis, *ibid.* **29**, 1453 (1984).

[8] S. Hess, Phys. Rev. A **22**, 2844 (1980); Physica A **118**, 79 (1983).

[9] (a) B. C. Eu, Ann. Phys. (N.Y.) **118**, 187 (1979); (b) J. Chem. Phys. **74**, 6362 (1981); (c) **87**, 1220 (1987).

[10] B. C. Eu and Y. G. Ohr, J. Chem. Phys. **81**, 2756 (1984).

[11] B. C. Eu, Phys. Fluids **28**, 222 (1985).

[12] R. E. Khayat and B. C. Eu, Phys. Rev. A **38**, 2492 (1988).

[13] B. C. Eu, Am. J. Phys. **58**, 83 (1990).

[14] T. L. Hill, *Statistical Mechanics* (McGraw-Hill, New York, 1956).

[15] J. P. Hansen and I. R. McDonald, *Theory of Simple Liquids* (Academic, London, 1986).

[16] J. Percus and G. J. Yevick, Phys. Rev. **110**, 1 (1958).

[17] G. S. Rushbrooke and H. I. Scoins, Proc. R. Soc. London, Ser. A **216**, 203 (1953); L. Verlet, Nuovo Cimento **18**, 77 (1960).

[18] J. F. Lustko, J. W. Dufty, and S. P. Das, Phys. Rev. A **39**, 1311 (1989).

[19] (a) W. Dreyer, J. Phys. A **20**, 6505 (1987); (b) D. Jou, C. Pérez-García, and J. Casas-Vásquez, *ibid.* **17**, 2799 (1984); (c) G. M. Kremer, Ann. Inst. Henri Poincaré, **45**, 419 (1986).

[20] J. G. Kirkwood, J. Chem. Phys. **3**, 300 (1935).

[21] B. C. Eu and H. H. Gan, Physica A **171**, 265 (1991).

[22] G. F. Mazenko and S. Yip, in *Statistical Mechanics,* edited by B. J. Berne (Plenum, New York, 1977), Part B.

[23] C. G. Gray and K. E. Gubbins, *Theory of Molecular Fluids* (Clarendon, Oxford, 1984), Vol. 1.

[24] (a) D. K. Bhattacharya and B. C. Eu, Mol. Phys. **59**, 1145 (1986); (b) Phys. Rev. A **35**, 4850 (1987); (c) B. C. Eu and R. E. Khayat, Rheol. Acta **30**, 204 (1991).

[25] R. B. Bird, R. C. Armstrong, and O. Hassager, *Dynamics of Polymeric Fluids* (Wiley, New York, 1977), Vol. 1, p. 141

[26] W. T. Ashurst and W. G. Hoover, Phys. Rev. A **11**, 658 (1975).

[27] G. Arfken, *Mathematical Methods for Physicists,* 2nd ed. (Academic, London, 1970), p. 224.

[28] N. G. van Kampen, *Stochastic Processes in Physics and Chemistry* (North-Holland, Amsterdam, 1990).

[29] M. E. Rose, *Elementary Theory of Angular Momentum* (Wiley, New York, 1957).

[30] L. Blum, J. Chem. Phys. **57**, 1862 (1972).

[31] P. T. Cummings, J. Ram, R. Barker, C. G. Gray, and M. S. Wertheim, Mol. Phys. **48**, 1177 (1983).

[32] F. Lado, J. Comp. Phys. **8**, 417 (1971).

[33] D. J. Evans, Physica A **118**, 51 (1983).

[34] K. Kawasaki and J. Gunton, Phys. Rev. A **8**, 2048 (1973).

[35] M. H. Ernst, B. Cichocki, J. R. Dorfman, J. Sharma, and H. van Beijeren, J. Stat. Phys. **18**, 237 (1978).

[36] J. H. Irving and J. G. Kirkwood, J. Chem. Phys. **18**, 817 (1950).

[37] J. Gómez Ordóñez, J. J. Brey, and A. Santos, Phys. Rev. A **41**, 810 (1990).